

RESEARCH ARTICLE

10.1002/2017WR021765

Effective Representation of River Geometry in Hydraulic Flood Forecast Models

S. Grimaldi¹ , Y. Li¹ , J. P. Walker¹ , and V. R. N. Pauwels¹ 

¹Department of Civil Engineering, Monash University, Clayton, VIC, Australia

Key Points:

- This paper presents a data-parsimonious methodology for the effective representation of river geometry in hydraulic flood forecast models
- A rectangular, width-varying shape with uniform longitudinal slope defined using remote sensing data and a few measurements is recommended
- Remote sensing-derived water level retrieved at the early stages of a flood can support detection of river geometry representation errors

Correspondence to:

S. Grimaldi,
stefania.grimaldi@monash.edu

Citation:

Grimaldi, S., Li, Y., Walker, J. P., & Pauwels, V. R. N. (2018). Effective representation of river geometry in hydraulic flood forecast models. *Water Resources Research*, 54. <https://doi.org/10.1002/2017WR021765>

Received 28 AUG 2017

Accepted 30 JAN 2018

Accepted article online 1 FEB 2018

Abstract Bathymetric data are a critical input to hydraulic models. However, river depth and shape cannot be systematically observed remotely, and field data are both scarce and expensive to collect. In flood modeling, river roughness and geometry compensate for each other, with different parameter sets often being able to map model predictions equally well to the observed data, commonly known as equifinality. This study presents a numerical experiment to investigate an effective yet parsimonious representation of channel geometry that can be used for operational flood forecasting. The LISFLOOD-FP hydraulic model was used to simulate a hypothetical flood event in the Clarence catchment (Australia). A high-resolution model simulation based on accurate bathymetric field data was used to benchmark coarser model simulations based on simplified river geometries. These simplified river geometries were derived from a combination of globally available empirical formulations, remote sensing data, and a limited number of measurements. Model predictive discrepancy between simulations with field data and simplified geometries allowed an assessment of the geometry impact on inundation dynamics. In this study site, the channel geometrical representation for a reliable inundation forecast could be achieved using remote sensing-derived river width values combined with a few measurements of river depth sampled at strategic locations. Furthermore, this study showed that spatially distributed remote sensing-derived inundation levels at the very early stages of a flood event have the potential to support the effective diagnosis of errors in model implementations.

Plain Language Summary Floods are among the most frequent and destructive natural disasters worldwide. An accurate and reliable flood forecast can provide vital information for land management and emergency response. Flood forecasts are achieved using numerical models that are able to predict the depth, velocity, and arrival time of the flood wave at each point of the valley. The accuracy of these predictions is strongly related to the quality of the three-dimensional representation of the valley. In particular, information on river geometry (that is cross-section shape, depth, and width) is critical to the application of these numerical models. However, it is impossible to measure river geometry along the entire river length, especially in large basins. This study developed a method to represent river geometry using a limited amount of time and money. Specifically, this objective can be achieved using available satellite imagery complemented with a few measurements. Moreover, this study showed that flood forecast skill can be improved by combining information from satellite and numerical models. Albeit simple, the river geometry representation proposed in this study can support the accurate prediction of floodplain inundation. This method was described and tested using, as example, a hypothetical flood event in an Australian catchment.

1. Introduction

Fluvial flooding is one of the most frequent and destructive natural disasters worldwide (CRED & UNISDR, 2015; De Groeve et al., 2015). An accurate and reliable flood forecast provides vital information for land management and emergency response. Consequently, operational flood forecasting systems should model runoff generation, runoff concentration, streamflow propagation, and floodplain inundation (Sene, 2008). Hydrological models, a component of the flood forecasting system, predict runoff generation and concentration from rainfall forecasts. A number of operational hydrological models have been developed over the last few decades (Pagano et al., 2014), and it has been shown that forecast accuracy of these models can be improved using remotely sensed soil moisture data (Li et al., 2016). Hydraulic models then take the

hydrologic model outflow hydrograph to compute water level and velocity in the river network, and when the storage capacity of the river is exceeded, in the floodplain. Remote sensing (RS) observations from radar altimeter, active synthetic radar, and optical instruments have been increasingly used to support hydraulic model implementation, calibration, and validation. Moreover, assimilation of RS data into hydraulic models has the potential to improve flood forecast skill in near real time (Grimaldi et al., 2016). The increased availability of RS data has allowed a number of applications at the continental to global scales (e.g., Sampson et al., 2015; Schumann et al., 2013; Yamazaki et al., 2013). However, only few operational systems currently incorporate the forecasting of floodplain inundation at the local scale (Dewelde et al., 2014).

Flood warnings at the local scale should be detailed and specific to the site and local conditions. For this reason, the implementation of hydraulic models demands for high-resolution and high accuracy data sets (Alferi et al., 2016; Perez et al., 2016). In particular, river bathymetric data are essential for the accurate modeling of river hydraulics, which is pivotal for the prediction of floodplain inundation (Neal et al., 2015; Trigg et al., 2009). Three-dimensional surfaces of river corridors can be reconstructed using point cloud data collected by multibeam sonars mounted to boats (e.g., Conner & Tonina, 2014) or cross sections surveyed with single beam sonars mounted to small watercraft (e.g., Pasternack & Senter, 2011). However, bathymetric data are not available for many rivers in the world (García-Pintado et al., 2015; Wood et al., 2016). Furthermore, even at the catchment scale, it is not economically and practically feasible to measure along the total length of a number of streams, especially considering that changing inputs of water, sediment, and vegetation often lead to alterations of river morphology over short time scales. In particular, moderate annual peak floods lead to altered cross-sectional geometry while rare infrequent events cause significant channel change (Buffington, 2012; Soar et al., 2017).

Remote sensing techniques can be used to assess river width, but river depth and channel shape cannot be systematically observed remotely (e.g., Alsdorf et al., 2007b; Sampson et al., 2015). In fact, river depth assessment from reflectance data measured by satellite or airborne optical instruments, or airborne bathymetric LiDAR, is limited to nearly clear shallow water (e.g., Kinzel et al., 2013; Legleiter, 2015; Legleiter et al., 2009; Pan et al., 2015). In the context of data scarcity, many studies have coupled data assimilation, inversion or calibration algorithms with hydraulic models to estimate river bathymetry from observations of water level or flood extent. In these algorithms, a first approximation of depth values is often derived from empirical equations relating river geometry to the catchment area (Leopold & Maddock, 1953). Observations of water levels can be provided by satellite altimeters. However, the coarse spatial (\sim km) and temporal (\sim months) sampling resolution of currently available products (e.g., ERS-2, ENVISAT, Jason-1-2-3, Sentinel 3A) may impede their application to riverine flood modeling in many catchments worldwide (Schumann et al., 2015). While higher temporal resolution water level time series for medium to large rivers can be potentially achieved by combining several years of observations from multiple sensors (Tourian et al., 2016), many researchers (e.g., Durand et al., 2008, 2014; Frasson et al., 2017; Garambois & Monnier, 2015; Mersel et al., 2013; Yoon et al., 2012) are looking at the potential of the upcoming Surface Water & Ocean Topography (SWOT) wide swath altimetry satellite mission to tackle the problem at coarse spatial resolution. The SWOT mission will provide spatial water level fields for all rivers wider than 100 m, with 10 cm water level accuracy over 1 km². This means, for instance, a 10 km reach for a river of 100 m width (Biancamaria et al., 2016; Rodriguez, 2015). However, questions on the feasibility of using 10 km averaged SWOT water level observations for many local-scale investigations (e.g., Biancamaria et al., 2010; Garambois & Monnier, 2015) can only be answered after the mission launch, currently expected in 2021 (<https://swot.jpl.nasa.gov/>).

Alternatively, water extent, levels, and slope can be retrieved from existing Synthetic Aperture Radar (SAR) and optical remote sensing. For instance, high-resolution optical data and high and coarse resolution SAR images were used by Durand et al. (2014), García-Pintado et al. (2015), and Wood et al. (2016) in data assimilation and calibration algorithms to simultaneously estimate channel geometry and roughness of the rivers Severn (UK) and Ohio (USA). However, it was shown that channel geometry and roughness compensate for each other with different parameter sets mapping model predictions to the observed data equally well, generating an equifinality problem. While this equifinality problem could have a limited impact on the modeling of large shallow rivers such as the Amazon River (Durand et al., 2008), it is highly relevant at small to medium scales, even when assimilating precise water elevation and slope data collected by a drifting GPS buoy into a hydraulic model (Hostache et al., 2015). In these cases, it was shown that use of (i) at least one field water depth measurement, (ii) a reduced range for roughness, or if available (iii) a good range of

flood magnitudes, could reduce the uncertainty in the identification of effective depth-roughness pairs within a rectangular channel implementation (Durand et al., 2014; Garambois & Monnier, 2015; García-Pintado et al., 2015; Wood et al., 2016). In fact, Neal et al. (2015) pointed out that geometry and friction had different impacts on flood dynamics when using a rectangular geometry where depth-roughness pairs were defined to match observed data at the local level, leading to spurious inundation predictions in the downstream area. Consequently, it was suggested that a more realistic representation of channel shape has the potential to lead to more robust solutions for model calibration.

The need for the inclusion of channel morphology in the model structure combined with the persistent problem of data scarcity demands cost-effective solutions for the assessment of river bathymetry. This study investigated the problem of implementing operational flood forecasting hydraulic models with limited field data. In many inhabited catchments sparse field data might be readily available, and local stakeholders could be willing to invest limited resources in field data collection but are not able to provide detailed bathymetric data. Consequently, this paper aims at providing advice on data collection and a method for the preliminary assessment of river bathymetry which is flexible (that is, applicable to any river width), parsimonious and repeatable over time. The resulting model implementation has to be effective. That is, it has to support appropriate inundation process representation. The impact of a different representation of river morphology on model predictions is likely to be a function of model structure, and the effective description of river geometry should be identified within the selected numerical framework. For instance, more complex geometrical representations might be required to compensate for the approximations of simplified numerical models (e.g., Fewtrell et al., 2011; Trigg et al., 2009).

Spatially distributed hydraulic flood forecasting models can be broadly distinguished as either full solutions of the shallow water equations (hydrodynamic or dynamic models) or simplified approximations in which the convective acceleration term in the momentum conservation equation is neglected (inertial approximation); both the convective acceleration term and the local acceleration term are neglected (diffusive approximation); or the pressure gradient and both the acceleration terms are neglected (kinematic approximation; Bates et al., 2010; Hunter et al., 2007). Only few studies have addressed the issue of representing channel complexity and type of numerical channel solver. Orlandini and Rosso (1998) showed that incorporating estimated channel geometry into a diffusion wave routing scheme based on the Muskingum-Cunge method produced a significant improvement in the description of the flood hydrograph at the outlet of the Sieve catchment (Italy) with respect to a less detailed network parameterization based on rectangular cross sections. Trigg et al. (2009) compared a one-dimensional (1-D) diffusive model (1-D-2-D LISFLOOD-FP, Bates & De Roo, 2000) based on simplified rectangular cross sections, with a hydrodynamic 1-D model (HEC-RAS, USACE) based on a fully irregular channel. They showed that channel water levels in large, shallow sloped rivers, such as the Amazon River, could be adequately reproduced using a prismatic rectangular channel having equivalent flow area as the real channel. However, floodplain water levels cannot be assumed to be the same as channel water levels and a detailed two-dimensional (2-D) modeling of the complex nonlinear interactions between the channel and floodplain is essential (Alsdorf et al., 2007a; Trigg et al., 2009). Fewtrell et al. (2011) compared the skill of complex, fully irregular geometries and simplified rectangular geometries embedded in a coupled 1-D-2-D hydrodynamic model (ESTRY-TUFLOW; Syme, 1991) for the prediction of gauged water levels and spatially distributed wrack marks in the Eden-Petteril-Caldew river system (United Kingdom). They concluded that accurate estimates of the river conveyance capacity and cross-section depth values were required for the predictions of far-field flood elevations within a fully hydrodynamic model framework. However, the same authors suggested that a more complex physical representation of the channel geometry could be necessary when model physical complexity is decreased.

The objective of this paper is the investigation of a parsimonious method for assessing river geometry requirements for effective implementation in operational flood forecasting systems. A 2-D modeling framework was deemed appropriate for this purpose. Even though 1-D codes are computationally very efficient, they cannot adequately simulate lateral floodplain wave routing (e.g., Alsdorf et al., 2007a; Hunter et al., 2007; Trigg et al., 2009). A numerical experiment was conducted by using the 2-D inertial model LISFLOOD-FP (Bates et al., 2010) to simulate a hypothetical flood event in a 20 km long meandering reach of the Clarence River (Australia). Despite LISFLOOD-FP having been widely used in riverine flood modeling studies, there has not been a thorough analysis of the impact that the channel geometry has on floodplain inundation patterns (Savage et al., 2016b). A high-resolution model based on accurate bathymetric field data was

used to benchmark coarser model simulations based on simplified representations of river geometry. Synthetic water level time series and RS-derived inundation extent and level were derived from the benchmark model and used for model verification and evaluation. The simplified river geometries were first derived from an analysis of the complete bathymetric field data set in order to investigate the level of river geometrical complexity required for the prediction of inundation dynamics within the selected numerical framework and study area. A number of geometrical representations were then hypothesized based on a combination of globally available empirical formulations, remote sensing data, and a limited number of measurements (that is, a small subset of the bathymetric field database). The a priori knowledge of the discrepancy between field data and simplified models allowed the impact of river geometry error on inundation modeling to be discussed. This numerical experiment illustrated the potential value of RS-derived inundation level for the diagnosis of errors in river geometry representation.

2. Test Site

The test site is the Clarence catchment (Australia, Figures 1a and 1b). The Clarence River is 394 km long and has a drainage area of 22,700 km². This catchment was affected by major floods in 2009, 2011, and 2013. The numerical model was setup to simulate a 21.3 km long river reach between Copmanhurst and Mountain View (Figure 1d), for which bathymetric data were available. This river reach is laterally stable,

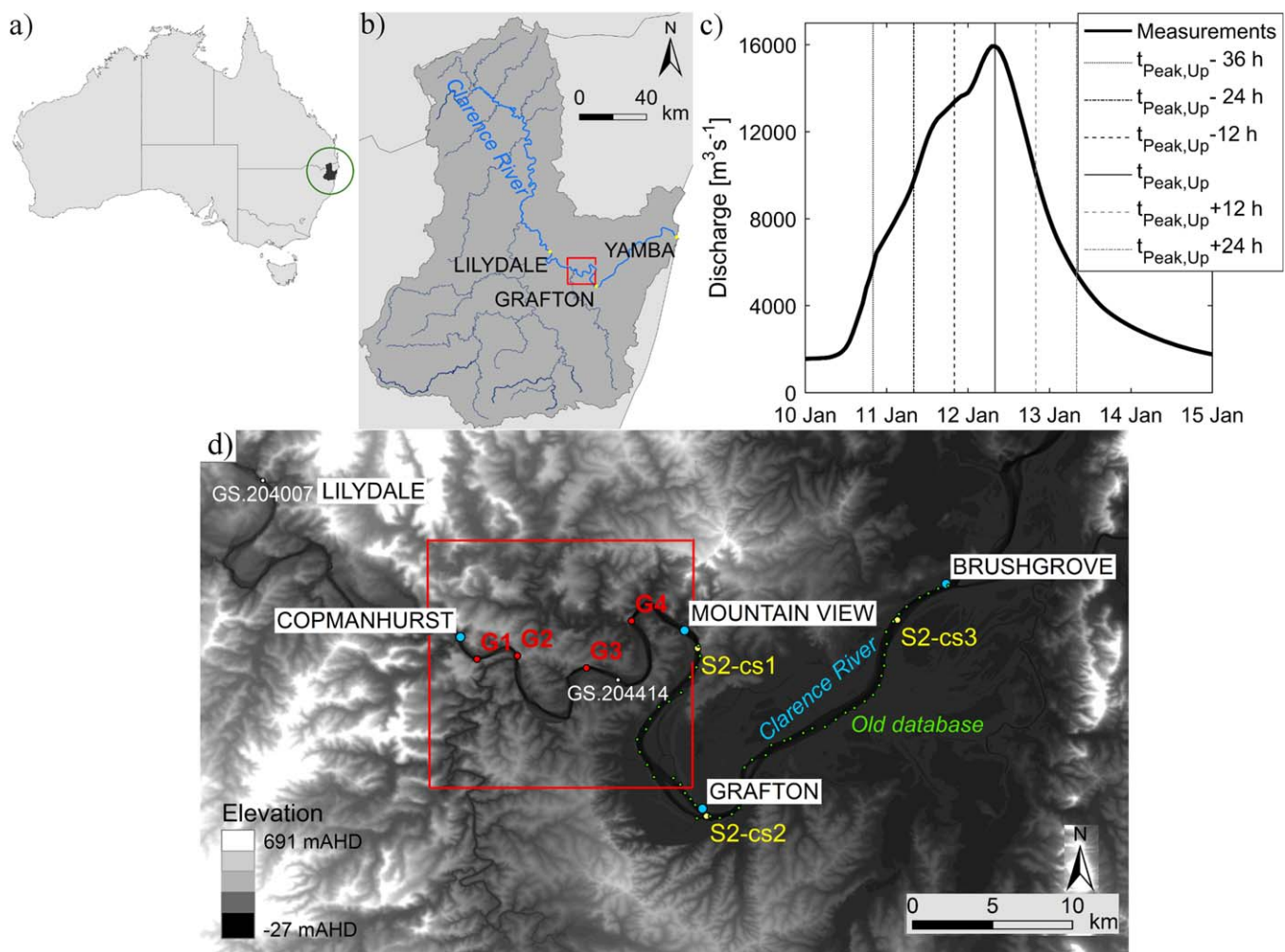


Figure 1. (a) Location of the Clarence catchment. (b) Clarence catchment, main towns. (c) Measured input discharge hydrograph at GS.204007. (d) Modeled area represented by the red square. Red points: synthetic water level gauges G1, G2, G3, and G4 (section 5.4). Yellow points: selected cross sections in scenario S2 (section 5.1). Green points: cross sections of the Old database (section 3).

unconfined, and meandering with sinuosity of 2 (Erskine et al., 2006). Lateral floodplains are steep and the valley is nearly V shaped. Flood events are quick in the area. For instance, in 2011 the flood peak travelled the 125 km from Lilydale to Yamba in less than 30 h with widespread flooding affecting all the urban areas along the Clarence River.

3. Field Data

River bathymetry can be effectively interpolated from cross sections surveyed with traditional survey equipment for wadeable streams (e.g., Waddle, 2010) or with sonar equipment mounted on small boats for non-wadeable reaches (e.g., Altenau et al., 2017). The accuracy of interpolated bathymetries depends on measurement error, the density and distribution of cross-section data, and the interpolation method (Glenn et al., 2016). Albeit inevitable, measurement errors can be accurately estimated. For this study, cross-section location and data analysis methods were defined following the guidelines presented by many authors (e.g., Castellarin et al., 2009; Conner & Tonina, 2014; Cunge et al., 1980; Samuels, 1990). Primary cross sections were placed at the beginning and end of the main geomorphologic features (restrictions, widenings, islands, bends, inflection points, and apexes of meanders were identified by a visual analysis of Google Earth) with an average spacing less than 2 km (Cunge et al., 1980). Secondary cross sections were drawn by applying a minimum spacing of 200 m (Conner & Tonina, 2014).

The field survey was completed in November 2015 using a SonTek M9 HydroSurveyor Acoustic Doppler Profiler mounted on a kayak. The M9 has built-in compensation for pitch and roll, and an integrated Differential Global Positioning System (DGPS) positioning solution with a horizontal accuracy of 1 m or less. Whenever possible, diagonal survey routes were used beside perpendicular cross sections in order to collect as much detail of the three-dimensional channel morphologic variability as possible (Figure 2a). Vertical profiles of salinity, temperature, and pressure were sampled using the Sontek CastAway and interpolated in space and time using HydroSurveyor software in order to achieve a full sound speed compensation of depth data and thus a 0.02 m depth accuracy (Figures 2a and 2b). The final database consisted of 59 cross sections having a mean distance of 350 m and a total of over 46,000 additional soundings. This database will be hereafter referred to as the Hi-RA (high-resolution and accuracy) database.

Sonar depths were converted to bed elevations and tied to the Australian Height Datum (AHD) using a planar water surface level fitted to water elevation records registered at Lilydale (Australian Bureau of Meteorology), Rogan Bridge, and Grafton (New South Wales Manly Hydraulics Laboratory). Each cross section was connected to the floodplain with the aid of a 1 m Lidar Digital Elevation Model (DEM) having a vertical accuracy of ± 30 cm and horizontal accuracy of ± 80 cm (New South Wales Land and Property Management Authority, 2010; Figure 2c). Following the recommendations by Glenn et al. (2016), a custom interpolation method based on a local along-thalweg curvilinear coordinate system was implemented to transform the irregularly spaced cross sections into a surface. This preliminary reconstruction of the riverbed surface was then modified to include the additional soundings using a second order inverse distance algorithm. The nearest neighbor method was finally used to sample this submeter irregular mesh topography to a regular 1 m grid which was integrated with the Lidar data into one seamless data structure (hereafter called 1mLIDAR-BATH).

A bathymetric survey of the Clarence River from Mountain View to Brushgrove (~ 41 km, green dots in Figure 1d) was completed in the 1960s. This database, which will hereafter be referred to as the Old database, includes 59 cross sections measured with an average spacing of 727 m. It was provided to the authors by BMT-WBM (Huxley & Farr, 2013). Information on the observation method and accuracy was not available (B. Rodgers, BMT WBM Pty Ltd, personal communication, 2016).

4. Data Analysis

4.1. Analysis of the Geometry of the Cross Sections at Bankfull Level

Flow levels change over time and channel limits cannot be defined by the wetted area at the time of measurement. Conversely, bankfull level, or the point at which the flow begins to enter the active floodplain (Leopold & Maddock, 1953), is a consistent benchmark for comparison between sites (Vermont Agency of Natural Resources, 2009). Bankfull flow area is consequently defined as the cross-sectional area of a channel

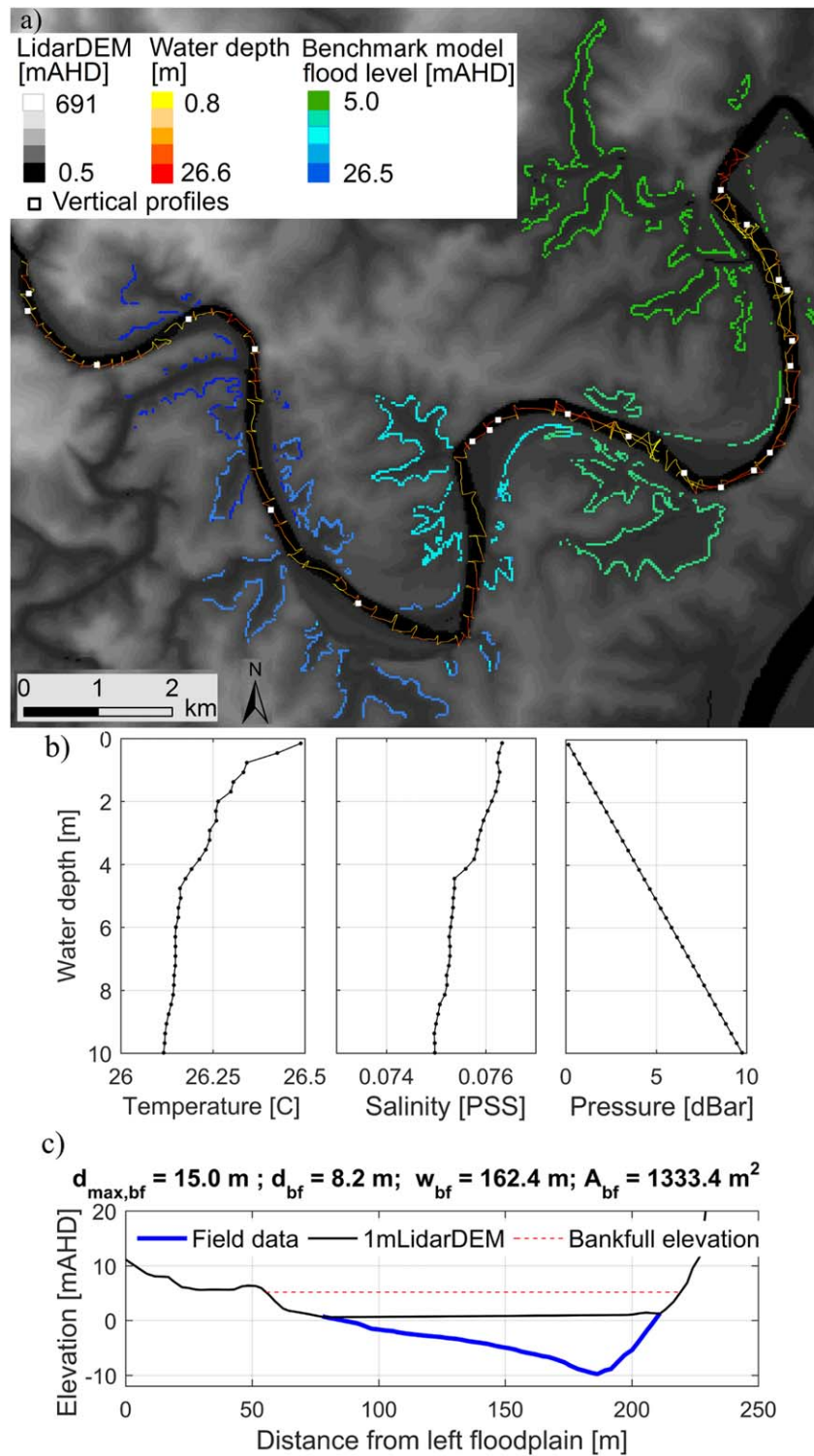


Figure 2. Hi-RA database spatial domain. (a) Location and value of the depth measurements; location of the vertical profiles. Hydraulic model results: water levels at flood peak as predicted by the benchmark high-resolution model (section 5.3). (b) Example of measured vertical profiles of water temperature, salinity, and pressure. (c) Example of a measured cross section. $d_{bf, \max}$, maximum bankfull depth; d_{bf} , bankfull depth; A_{bf} , bankfull flow area; w_{bf} , bankfull depth (section 4.1).

Table 1a
Bankfull Parameters of the Hi-RA Database (59 Cross Sections)

Hi-RA database	w_{bf} (m)	$d_{bf,max}$ (m)	d_{bf} (m)	A_{bf} (m ²)	s
Median	213.3	11.7	6.7	1,498.1	1.7
Mean	224.6	11.6	7.1	1,598.7	2.1
Standard deviation	52.6	4.0	2.1	406.9	1.3
Minimum	132.1	5.5	3.8	1,014.5	0.6
Maximum	365.6	24.1	13.7	2,794.3	6.5

Table 1b
Bankfull Parameters of the Old Database (59 Cross Sections)

Old database	w_{bf} (m)	$d_{bf,max}$ (m)	d_{bf} (m)	A_{bf} (m ²)	s
Median	553.0	9.6	5.7	2,987.3	1.5
Mean	509.6	10.7	6.4	2,938.5	1.7
Standard deviation	141.1	4.2	2.0	376.0	0.9
Minimum	204.0	5.5	3.7	1,989.2	0.5
Maximum	792.0	27.1	13.3	3,728.5	5.6

Table 1c
Comparison Between the Bankfull Parameters of the Five Cross Sections Common to the Hi-RA and Old Database

Hi – RA database	$\frac{w_{bf,Hi-Ra}}{w_{bf,Old}}$	$\frac{d_{bf,max,Hi-Ra}}{d_{bf,max,Old}}$	$\frac{d_{bf,Hi-Ra}}{d_{bf,Old}}$	$\frac{A_{bf,Hi-Ra}}{A_{bf,Old}}$	$\frac{S_{Hi-Ra}}{S_{Old}}$
Old database					
Mean	1.20	0.96	0.97	1.30	1.2
Standard deviation	0.05	0.01	0.01	0.05	0.02

Note. w_{bf} , bankfull width; $d_{bf,max}$, maximum bankfull depth; d_{bf} , bankfull depth; A_{bf} , bankfull flow area; s , shape coefficient.

just before floodplain flooding occurs. In this study, bankfull level was identified using a combination of indicators including geometrical break from steep slope to gentle slope; erosional features; and change in vegetation (e.g., Dingman, 2009; Rosgen, 1996). Estimated bankfull levels were 5.5 m AHD at Copmanhurst and 2.8 m AHD at Mountain View with a longitudinal slope of 0.13‰. Table 1a shows the geometrical features of the Hi-RA database. Bankfull width (w_{bf}) ranges between 132 and 365 m (with a mean value of 224 m). Maximum bankfull depth ($d_{bf,max}$) was identified by the lowest point of the cross section, that is the thalweg (e.g., De Rose et al., 2008). Its value varies between 5 and 24 m (with a mean value of 11.6 m) and it is on average 63% higher than the mean channel depth or bankfull depth (d_{bf} , computed as the ratio between bankfull flow area A_{bf} and bankfull width) thus revealing that most of the cross sections are far from rectangular. For each cross section, Figure 3a shows the distance of the left and right bank from the thalweg. The distances were normalised to the bankfull width. Since a symmetrical cross section would be described by -0.5 and $+0.5$ values, Figure 3a shows the distinctive nonsymmetrical shape of most of the measured cross sections. Analytical models for the description of nonsymmetrical cross-section shapes are not known to the authors. For this reason, a general symmetrical cross-section shape model has been used (e.g., Dingman, 2009; Neal et al., 2015). In this model, the channel shape can be described using a simple dimensionless shape coefficient s computed by fitting the exponential relationship between channel flow width w and depth d values normalised to the bankfull values according to

$$\frac{w}{w_{bf}} = \left(\frac{d}{d_{bf}} \right)^{\frac{1}{s}} \quad (1)$$

As shown in Table 1a and Figure 3b, cross-section shapes along the river reach could alternatively be concave ($s < 1$), triangular ($s = 1$), parabolic ($s = 2$), or almost rectangular ($s \gg 5$).

Five cross sections were common to the Hi-RA and Old database. Each pair of cross sections was compared by computing the ratio of the bankfull parameters (w_{bf} , d_{bf} , $d_{bf,max}$, A_{bf} , s); values close to 1 (Table 1c) suggested a limited morphological variability of the river reach over the last fifty years. Similarly to Table 1a, Table 1b shows that the cross sections of the Old database are characterised by a large variety of shapes, mostly not rectangular. Moreover, when compared to the Hi-RA database, the cross sections of the Old database have a similar range of depth values but higher values of width leading to larger values of flow area.

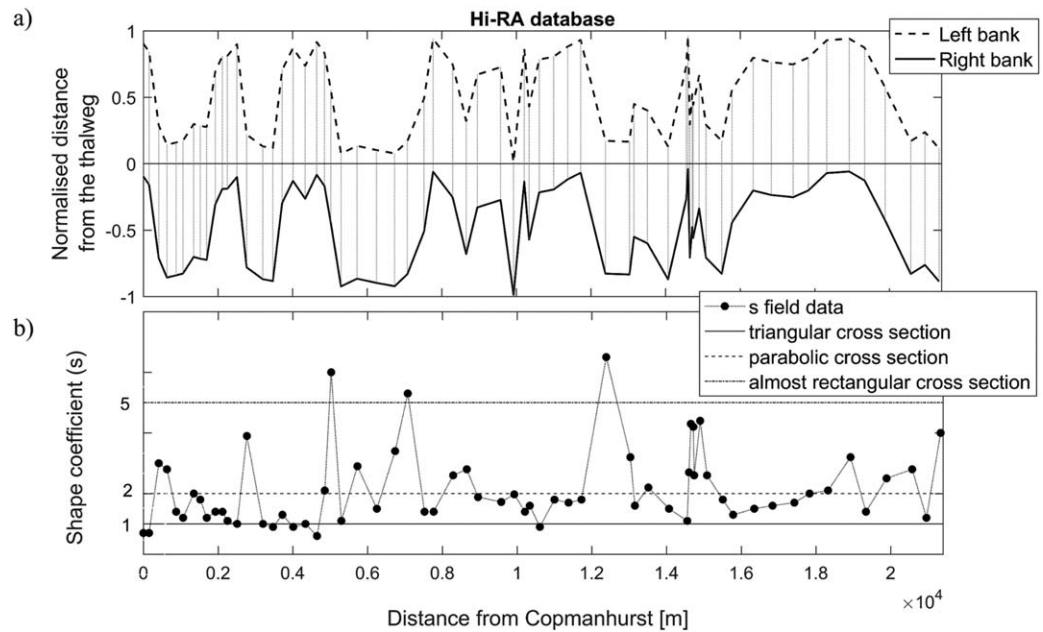


Figure 3. Hi-RA database: (a) distance of each bank from the thalweg, the values are normalized to the bankfull width; (b) shape coefficient s .

4.2. Remote Sensing and Empirical Databases of Bankfull Parameters

Modeling of the river network requires channel centerlines, flow direction data, a river mask, a set of depth values, and information on river shape. Channel centerlines and flow directions can be derived from the morphological analysis of DEMs. Near-global and continental scale databases, such as the 3 arc sec (~ 90 m at the Equator) resolution flow direction data layer and the 15 arc sec (~ 500 m at the Equator) river network data layer included in the HydroSHEDS (Lehner et al., 2008; Lehner & Grill, 2013) and the 9 arc sec (~ 270 m at the Equator) resolution Australian Hydrological Geospatial Fabric (Australian Bureau of Meteorology, 2015, <http://www.bom.gov.au/water/geofabric/index.shtml>), are readily available. River masks are generally retrieved from optical remote sensing images. For instance, Altenau et al. (2017) used 5 m resolution RapidEye images; O’Loughlin et al. (2013) and Yamazaki et al. (2015) used a set of 30 m resolution Landsat images. In Australia, the web service Water Observation from Space (WOfS, Geoscience Australia, <http://www.ga.gov.au/scientific-topics/hazards/flood/wofs>) provides a statistical analysis of surface water observations derived from Landsat imagery (Mueller et al., 2016). In particular, permanent water bodies are identified by pixels having observed water recurrence equal or higher than 80% (Mueller et al., 2016). River masks can be integrated with channel centerlines and flow direction data to estimate river width. Semiautomatic (e.g., O’Loughlin et al., 2013; Pavel-sky & Smith, 2008; Trigg et al., 2012) or fully automatic (e.g., Sampson et al., 2015; Yamazaki et al., 2014) algorithms have been developed for this purpose and their application allowed the delivery of regional to global databases, such as the 1 arc sec (~ 30 m) resolution North America River Width data set (Allen & Pavel-sky, 2015) and the 3 arc sec (~ 90 m) resolution Global Width Database for Large Rivers (Yamazaki et al., 2014).

As an alternative to the use of remote sensing data, bankfull width values can be derived from a set of empirical geomorphic relationships known as the *at-a-station* hydraulic geometry relations, introduced by Leopold and Maddock (1953), and widely used in literature (e.g., Camporese et al., 2010). In these equations bankfull width (w_{bf}) and depth (d_{bf}) are expressed as a power function of bankfull discharge (Q_{bf}) which can be assessed by local flood analysis or as a power function of the catchment drainage area (A_c) according to

$$w_{bf} = aQ_{bf}^b, \tag{2a}$$

$$d_{bf} = cQ_{bf}^f, \tag{2b}$$

$$Q_{bf} = kA_c^h. \tag{2c}$$

Table 2
RS-Derived Database and the At-A-Station Formulations for Assessment of the Bankfull Parameters

Catchment area	Near global: e.g., HydroSHEDS (Lehner et al., 2008) Australia: GEOFABRIC	
↓		
Discharge at bankfull	Empirical formulations Near global: e.g., Andreadis et al. (2013) Australia: e.g., Gordon (1996)	
↓		
Depth and width	Near global: e.g., Moody and Troutman (2002) Australia: e.g., Stewardson (2005) and De Rose et al. (2008)	← RS-derived width database Near global: Global Width Database for Large Rivers (Yamazaki et al., 2014) Australia: Water Observations from Space (Mueller et al., 2016)

The empirical coefficients a, c, k and exponents b, f, h of these equations are related to local climatic and geological conditions (Phillips, 1990), with possible similarities at the reach scale (Gleason & Wang, 2015). For instance, Gordon (1996), Stewardson (2005), Dingman (2007), Harman et al. (2008), and De Rose et al. (2008) proposed assessment methods for bankfull discharge and river geometry for many rivers in South-East Australia. These correlations were applied here for the prediction of bankfull geometry of the Clarence River. Empirical analyses are not available for each catchment worldwide and Andreadis et al. (2013) published a 15 arc sec (~450 m) resolution near-global river bankfull width and depth database. Bankfull values were derived from the application of a unique parameter set (Moody & Troutman, 2002) to a global power correlation between bankfull discharge and drainage area. The mean and the 5–95% confidence intervals were computed to account for the variability of rivers worldwide. This database (usually the mean values) has been widely used in river modeling (e.g., Sampson et al., 2015; Schumann et al., 2013). Table 2 shows the RS-derived database and the at-a-station formulations used in this study to provide a number of estimates of bankfull width and depth.

5. Methods

5.1. Numerical Model, Boundary Conditions, Parameters, Grid Size

The inertial formulation of the 2-D hydraulic model LISFLOOD-FP (Bates et al., 2010) was chosen for this study. This model has proved to be accurate against analytical solutions and hydrodynamic models (Néelz & Pender, 2013), while also being more computationally efficient than diffusive models (de Almeida et al., 2012). The numerical scheme is based on a finite difference method which is explicit in time and first order in space. Water flows Q are estimated separately through each face of a regular computational grid. For each direction (X and Y), the explicit form for the calculation of Q at the new time step ($t + \Delta t$) is given by

$$Q^{t+\Delta t} = \frac{q^t - g d^t \Delta t \frac{\Delta(d^t+z)}{\Delta x}}{\left(1 + g \Delta t n^2 |q^t| / (d^t)^{7/3}\right)} \cdot \Delta x, \quad (3)$$

where Q is the flow ($\text{m}^3 \text{s}^{-1}$), q is the flow per unit width ($\text{m}^2 \text{s}^{-1}$), g is the gravitational acceleration (9.81 m s^{-2}), d is the depth of flow (m), z is the river bed elevation (m), n is Manning's roughness coefficient ($\text{m}^{-1/3} \text{ s}$), and Δx is the cell resolution (m). The continuity equation is then applied to the full grid domain to update water depths inside each computational cell, thus achieving a 2-D solution. Numerical instabilities may arise at low Manning's n values (Bates et al., 2010) and this problem was solved by introducing the diffusive term proposed by de Almeida et al. (2012). However, these conditions do not arise in our model setups.

Implementation of the model requires a DEM, a description of river geometry, input and boundary conditions, and spatially distributed roughness coefficient values. Lateral tributaries and bridges were not

included in the model setup. The DEM used was the *1mLIDAR-BATH* and river geometry was discretized using a number of grid cells. Gauged data were not available at the upstream (Copmanhurst) and downstream (Mountain View) boundaries of the computational domain. Consequently, the discharge hydrograph measured at the closest upstream gauge station (GS.204007, Australian Bureau of Meteorology, Figure 1d) during the January 2011 flood (Figure 1c) was used as upstream boundary condition, and water levels measured during a low flow period at the closest gauge station to Mountain View (GS.204414, New South Wales Manly Hydraulics Laboratory, Figure 1d) were used as downstream boundary condition. This latter choice accounted for the relevant impact of tidal levels on riverine flow in this catchment; moreover, the induced backwater effects could enhance floodplain inundation and thus help identifying the discrepancies between model outputs for extreme flood events. A few model simulations were made with free slope boundary conditions to discard the hypothesis of a large impact of downstream boundary conditions on predicted flood extent and levels, and consequently on the overall conclusions of this modeling exercise.

In hydraulic modeling of floods, spatially distributed roughness coefficients are often disaggregated into two values only, one for the channel and the other for the floodplain (e.g., Werner et al., 2005) and considered as effective parameters used to compensate for lack of process and topographic representation (e.g., Horritt & Bates, 2001; Jung et al., 2012). In this study, channel Manning's roughness values were varied from 0.005 to 0.07 $\text{m}^{-1/3} \text{ s}$ with steps of 0.005. The floodplain Manning's roughness value was set to 0.035 $\text{m}^{-1/3} \text{ s}$ to represent the impact of high grass, crops, scattered brush, and scattered trees on surface flow (Chow, 1959) and kept constant for all the models; this choice allowed for a focus on the impact of channel roughness and geometry on model results.

Recent advances in code parallelization methods (e.g., Neal et al., 2010) and Graphical Processing Units (GPUs; e.g., Kalyanapu et al., 2011) have decreased computational time. However, multiple model runs at fine-scale might still be too computationally expensive, especially for operational purposes (Savage et al., 2016b). Consequently, topographic data are commonly resampled to a coarser grid than its original form, with the critical choice of spatial resolution usually the outcome of a site-specific compromise between computational time and model accuracy. Examples of results reported in literature are 50 m for the Imera catchment, Italy (Savage et al., 2016a), 120 m for the Thompson River, Australia (Jarihani et al., 2015), and 250 m for the Atchafalaya Basin, USA (Jung & Jasinski, 2015). In this study, the *1mLIDAR-BATH* was resampled using the Geo Editor for Modeling (Hilton, 2017) to create four DEMs having 5, 10, 30, and 90 m grid size, respectively.

5.2. Geometrical Representation of the River

5.2.1. Simplified Geometries Derived From the Field Data

A set of simplified geometries based on bankfull parameters of the Hi-RA database were hypothesized to investigate which geometrical features allow enough physical representation of flow dynamics in a meandering river within the selected numerical modeling frame. Four models (R1, R2, R3, and R4) had a rectangular shape; two models (E1 and E2) had an exponential shape. Model R1 was based on measured bankfull values of width and depth. This approach was used in previous studies (e.g., Fewtrell et al., 2011; García-Pintado et al., 2015; Neal et al., 2015; Trigg et al., 2009) to speed up model implementation while maintaining a certain level of river geometry variability. In model R1, channel longitudinal maximum bankfull depth variability is neglected. Conversely, model R2 used the measured maximum bankfull depth values while cross-section width was adjusted to maintain the measured cross-section flow area, as suggested by Fewtrell et al. (2011). Information on real cross-section shape was lost in both models R1 and R2. However, flow area was maintained at each cross section and the implementation of these models was limited to data-rich catchments. Models R3, R4, E1, and E2 maintained the consistency of flow area at the reach scale but could be applied to a larger number of catchments, where width data can be measured by remote sensing instruments and a limited number of measurements of river depth were available. Model R3 had a constant longitudinal slope derived from the linear interpolation of measured bankfull depth. Measured bankfull width values represented the inter-cross-section geometrical variability. Model R4 used a prismatic rectangular channel where bankfull width and depth values were derived from the linear interpolation of the field data. A prismatic, rectangular channel is the common assumption in many continental and global modeling exercises where only at-a-station empirical relationships are available (e.g., Schumann et al., 2016). The same interpolated values were used in models E1 and E2. Similarly to Neal et al. (2015) and Orlandini and Rosso (1998), the cross-section shape was conceived here as an additional calibration

Table 3
Simplified Geometrical Models Tested

Model notation	Shape	Width	Depth
R1	Rectangular $s \gg 5$	Measured cross-section values of w_{bf}	Measured cross-section values of d_{bf}
R2	Rectangular $s \gg 5$	Ratio of measured cross-section values of bankfull flow area and maximum depth: at each cross section $w = A_{bf} / d_{bf, \max}$	Measured cross-section values of $d_{bf, \max}$
R3	Rectangular $s \gg 5$	Measured cross-section values of w_{bf}	Linear interpolation of measured cross-section values of d_{bf}
R4	Rectangular $s \gg 5$	Linear interpolation of measured cross-section values of w_{bf}	Linear interpolation of measured cross-section values of d_{bf}
E1	Exponential $s = 2.1$	Linear interpolation of measured cross-section values of w_{bf}	Linear interpolation of measured cross-section values of d_{bf}
E2	Exponential $s = 1$	Linear interpolation of measured cross-section values of w_{bf}	Linear interpolation of measured cross-section values of d_{bf}

Note. w_{bf} , bankfull width; $d_{bf, \max}$, maximum bankfull depth; d_{bf} , bankfull depth; A_{bf} , bankfull flow area; s , shape coefficient.

parameter to improve the models physical accuracy and robustness. Model E1 used the median value of the modeled shape coefficients ($s = 2.1$; Table 1a); model E2 was based on triangular cross sections ($s = 1$). Table 3 provides a summary of the model setups. Simplified cross sections were used to replace the real ones and the river bathymetry was reconstructed using curvilinear interpolation.

5.2.2. Simplified Geometries in Data-Scarce Scenarios

Morphological variability along a river is the result of the combination of a plethora of climatic and geological factors. As a consequence, the modeling of bankfull parameters variability is extremely difficult (e.g., De Rose et al., 2008). At-a-station equations provide a parsimonious correlation with catchment area, yet a choice among the large variety of coefficients and exponents has to be made. In this paper, a simple approach to investigate the possibility of achieving an estimate of local river morphology was applied using a limited number of field data. RS and empirically derived values of bankfull parameters were computed as explained in section 4.2 (Table 2). These estimates were compared with the Hi-RA and Old databases using the ratio of the root-mean-square error to the standard deviation of measured data (RSR) and the percent bias (PBIAS).

Within the hypothesis of lack of field data from Copmanhurst to Mountain View (i.e., the domain of the hydraulic model), the bankfull parameters for the implementation of the simplified geometries were derived from an analysis of the Old database. Although sampling cross sections along the modeled river reach would be clearly advisable, this hypothesis allowed the assessment of the worst case scenario where data in the area of interest are not available. The results of the formulations listed in section 4.2 (Table 2) were compared to a subset of width, depth, and flow area values extracted from the Old database. The formulation that minimized the RSR value and the absolute value of PBIAS was used to reconstruct the geometry of the “unknown” river reach, from Copmanhurst to Mountain View. Three scenarios were hypothesized: S1 was based on the full Old database; S2 used three cross sections selected at strategic locations; and S3 used the three least representative cross sections. In S2, the three cross sections were selected a priori based on a visual analysis of Google Earth images. These cross sections were distributed along the reach from Mountain View to Brushgrove and showed different river width values (S2, cs1–2–3, Figure 1d). S3 was defined a posteriori based on the analysis of the full Old database. Simplified cross sections were used to replace the real ones and the river bathymetry was reconstructed using curvilinear interpolation.

5.3. Experimental Design

A high-resolution simulation based on the Hi-RA bathymetric database was considered as the benchmark to verify if coarse resolution models relying on simplified river geometries are consistent abstractions of the benchmark simulation. As stated in section 5.1, observed boundary conditions for the modeled domain were not available. Consequently, the high-resolution benchmark model does not attempt to represent the real system, but only a hypothetical system which is similar to the selected reach (e.g., Andreadis et al.,

2007). Moreover, accuracy is not necessarily increased by higher precision (Dottori et al., 2013; Savage et al., 2016b), and this study presents a sensitivity analysis undertaken by assessing coarse, simplified model predictions with respect to the data-rich benchmark solution (e.g., Fewtrell et al., 2008; Ozdemir et al., 2013; Yu & Lane, 2006).

Specifically, a model realization having 5 m grid size based on the Hi-RA bathymetric database, and with river Manning's roughness value of $0.03 \text{ m}^{-1/3} \text{ s}$ was considered as the benchmark. The selected river roughness value has been recommended for clean, full stage main channels, without rifts or deep pools (Chow, 1959). The benchmark model was used to generate synthetic time series of water level and synthetic maps of flood extent and level. Model verification was undertaken by assessing coarse model predictions of water level and extent with respect to the benchmark solution. Previous studies analyzed the sensitivity of LISFLOOD-FP outputs to the computational grid size (e.g., Horritt & Bates, 2001; Savage et al., 2016b). The testing of different grid sizes here was merely functional to the choice of the appropriate coarse grid size for operational purposes. Simplified geometrical representations of the river were therefore embedded in this coarse grid size. Albeit inevitable, topographic, and bathymetric uncertainties exert a dominant control on flooding patterns (Altenau et al., 2017) and, besides the decreased spatial resolution, even the method applied to produce the coarser DEM could affect model predictions (Fewtrell et al., 2008). In these cases, a relative comparison between the coarse yet data-rich model, and model implementations having the same grid size but based on simplified river geometries, is likely to provide relevant information on the impact of uncertainties in the river bathymetry representation on the predictive skill of the selected modeling frame. Information on errors in the representation of the real river geometry was then correlated to the loss of inundation prediction accuracy to investigate the impact of a poor knowledge of the river on flood inundation dynamics.

The analysis presented in this study required 182 model runs. The first model simulation was the high-resolution, data-rich benchmark model. Three coarser model resolutions (10, 30, 90 m; section 5.1) were then tested to identify the grid size for the analysis of the river geometry; each coarse model was implemented with 14 river roughness values totaling 42 model runs. The effectiveness of a number of simplified river geometries (section 5.2) in reproducing the benchmark model was then tested by inserting the simplified cross section into the selected coarse grid size. Bankfull parameters (i.e., width, depth, flow area, and shape) of the simplified river geometries were first derived from the Hi-RA database to understand how the model structure interacts with variations in river capacity, shape, and roughness. Six simplified geometries, namely R1, R2, R3, R4, E1, and E2 (section 5.2.1), were derived from the Hi-RA database and tested with 14 river roughness values, totaling 84 model runs. Measured bankfull parameters were then compared to estimates derived from RS data and at-a-station equations to suggest a data-parsimonious method for the preliminary assessment of river geometry according to three data-scarce scenarios, namely S1, S2, and S3 (section 5.2.2). Finally, four models were derived by combining selected river geometries and data-scarce scenarios. These 4 models were named R3-S1/S2, E-S1/S2, R3-S3, and E-S3; each of these models was tested with 14 river roughness values, totaling 56 model runs.

5.4. Performance Metrics

Due to the intrinsic nonlinearity of flood wave propagation, implementation factors (i.e., in this study, river geometry and roughness) affect different aspects of flood inundation processes in different ways and the magnitude of these impacts can vary in time and space (e.g., Fewtrell et al., 2011; Neal et al., 2015; Savage et al., 2016b). As such the choice of performance metrics can affect the outcomes of the model evaluation exercise. To the authors' best knowledge, a combined performance metric has not yet been proposed in literature. Conversely, the use of a number of performance measures was recommended to achieve a holistic evaluation of model accuracy (e.g., Pappenberger et al., 2007).

In this study, simplified model verification was undertaken by assessing model predictions of water level at the point scale and of inundation extent and level at the spatially distributed scale with respect to the benchmark solution. Gauged data of water level and/or discharge have been traditionally used to evaluate the skill of flood forecasting models at the point scale. However, it has recently been recognized that RS-derived spatially distributed information of water extent and levels offer more appropriate and comprehensive ways of comparison (e.g., Bates et al., 1997). An extensive research effort is being employed to investigate the recommended acquisition time and to reduce the uncertainties in RS-derived flood extent and level (e.g., Giustarini et al., 2016; Twele et al., 2016). These uncertainties might hinder the impact of RS data

in model calibration and evaluation exercises (Grimaldi et al., 2016). In this study, a number of error-free, synthetic RS observations were extracted from the high-resolution benchmark model before, at, and after the flood peak. Removing the uncertainty stemming from real field and RS data allowed a strict comparison of the outcomes of different model implementations.

Two performance metrics (specifically, root-mean-square error, RMSE, and flood peak ratio, PR) were used to assess model predictive skill at the point scale along the main channel, and two performance metrics (specifically, critical success index, CSI, and water level score, WLS) were used to assess model performance at the catchment scale, i.e., to assess model capability of predicting floodplain inundation. This choice allowed comparing the utility of point scale and spatially distributed performance metrics for model evaluation. RMSE and PR were used to compare modeled time series of water levels at four locations along the river (G1, G2, G3, and G4; Figure 1d) with the benchmark high-resolution simulation. The RMSE was selected to quantify the absolute discrepancy between modeled and benchmark values while the PR allowed a relative evaluation and an immediate detection of overestimation and underestimation errors. Spatially distributed flood extent and water level were compared at four lead times selected to represent different stages of the flood event (e.g., Savage et al., 2016a). Specifically, 24 and 12 h before the flood peak at the upstream boundary ($t_{Peak,Up}$), at $t_{Peak,Up}$, 12 h after $t_{Peak,Up}$ (the benchmark inundation extent was negligible 36 h before and 24 h after $t_{Peak,Up}$). The use of RS-derived inundation level is subjected to the availability of a high-resolution and accuracy DEM and the relative value of RS-derived flood extent and level to constrain the parameter space of hydraulic flood forecasting models has been the topic of recent investigations (Stephens & Bates, 2015; Stephens et al., 2014). Modeled flood extent maps were evaluated against those from the high-resolution benchmark solution using the *CSI* (Aronica et al., 2002) such that

$$CSI = \frac{A}{A+B+C}, \quad (4)$$

where *A* is the total area correctly predicted as flooded, *B* is the dry area incorrectly modeled as flooded, and *C* is the flooded area incorrectly modeled as dry. A cell was considered as flooded when water depth was equal to or greater than 0.10 m (e.g., Savage et al., 2016a). In order to account for the coarser spatial resolution of the simplified geometrical models, the number of flooded cell were counted according to the benchmark model within each coarse grid cell.

Synthetic RS-derived water level data were obtained by extrapolating the 5 m DEM elevation at each point of the flood margin as predicted by the benchmark high-resolution model. Due to the coarser resolution of the simplified geometrical models, a number of synthetic observations could fall into the same modeled grid cell. Large variation of flood margin elevation could be observed in steep slope areas of the 1m Lidar DEM. Consequently, as suggested by, e.g., Mason et al. (2012), synthetic water level observations could not fall in areas having a slope equal to or larger than 0.25 ($\sim 14^\circ$), with an enlarged exclusion area radius of 30 m. As an example, Figure 2a shows the water levels at time $t_{Peak,Up}$ as predicted by the high-resolution benchmark model. The application of a full protocol for the assessment of distributed values of water level was outside the scope of this paper, and so all the remaining points were retained for model evaluation. In particular, the minimum, midpoint, and maximum benchmark water levels were computed for each cell of any coarser model simulation. The performance measure used here was first introduced by Savage et al. (2016a). A water level point score (*WLpoint*, equation (5)) was computed for each water level observation extrapolated from the high-resolution benchmark model. The model scored 0 if the predicted water level was at the midpoint of the interval of the values predicted by the benchmark solution, ± 2 if the modeled water level was equal to two times the difference between the uncertainty bound and midpoint of the benchmark water level such that

$$WLpoint = \frac{\text{Modeled water level} - \text{Benchmark water level, midpoint}}{0.5(\text{Benchmark water level, maximum} - \text{Benchmark water level, minimum})}. \quad (5)$$

If a benchmark water level observation fell in a dry modeled cell, the modeled water level was retrieved from the nearest modeled wet cell (Neal et al., 2009). The overall *WLS* for a model simulation was given by the mean of the point scores such that

$$WLS = \frac{\sum_{i=1}^n \sqrt{WLpoint_i^2}}{n.obs}, \quad (6)$$

where n_{obs} is the number of observations. Finally, a simple graph reporting modeled water levels on the y axis and water levels predicted by the benchmark model on the x axis was used to analyze the model results at the spatially distributed scale. Good model predictions result in a set of points aligned along the 1:1 line.

6. Results and Discussion

6.1. Simplified Geometries Derived From the Field Data

Model accuracy and computational time decreased with increasing grid size (Table 4). For this study site, a 30 m grid size was a cost-effective modeling solution (0.34 m RMSE, 1.02 PR, 0.91 CSI, and 0.08 WLS). This model application is referred to herein as 30-Bath. A set of simplified river geometries was embedded into this coarse grid size (section 5.3). When evaluating medium to coarse model realizations in nearly V-shaped valleys, the uncertainty bound of high-resolution benchmark water levels, given by the difference between the maximum and the minimum benchmark water levels at fine resolution, might be as high as 2 m, and small values of WLS are expected (equation (6) and section 5.4). For this reason and as explained in section 5.3, the use of the 30-Bath data-rich model as an additional benchmark for the evaluation of data-parsimonious model implementations was considered of greater interest than the pursuit of higher model performances for this model.

Implementation of models R1-2-3-4, and E1-2 had 30 m grid size and was based on the Hi-RA database. Consequently, an overall agreement with the benchmark high-resolution model was expected. For each model setup, Table 5 shows the highest values of the performance metrics (RMSE, PR, CSI, and WLS) that were achieved when applying a simple tuning of the Manning’s river roughness coefficient (section 5.2).

The performances of model R1 and R2 at the point scale (R1: 0.35 m average RMSE, 0.99 average PR; R2: 0.73 m average RMSE, 0.97 average PR) and at the distributed scale (R1: 0.88 average CSI, 0.08 average WLS; R2: 0.88 average CSI, 0.12 average WLS) showed that a set of rectangular cross sections having equivalent flow area as the real channel can be used for the prediction of floodplain inundation when an inertial raster based numerical model is applied to a meandering river. R1 achieved a performance very similar to the model 30-Bath when using the same Manning’s roughness value as the high-resolution benchmark model. In model R2, the enhanced geometrical roughness due to the high variability of maximum cross-section depth values was compensated for by a smaller value of Manning’s surface roughness.

As explained in section 5.2.1, models R1 and R2 required detailed field measurements; conversely, models R3, R4, E1, and E2 were suitable for data sparse areas. The implementation of models R3 and R4 required RS-derived width data. Model R3 had the capability to reproduce the high-resolution benchmark model similar to the data demanding models R1 and R2. Conversely, model R4 had the lowest skill. The implementation of models E1 and E2 did not require RS-derived width data; model E1 was based on a more realistic representation of cross-section shape and led to more accurate representation of the benchmark model than model E2 based on a triangular channel. A thorough analysis of each model outcomes is presented hereafter. The results of model R3 (0.37 m average RMSE; 1.01 average PR; 0.90 average CSI; 0.09 average WLS) showed that, in this study site, and differently from Fewtrell et al. (2011), bankfull width variability

Table 4
Model Performance Metrics and Computational Time for Increasing Grid Size

Grid size (m)	Number of cells; computational time	RMSE Average of G1, G2, G3, G4 (m)	PR Average of G1, G2, G3, G4	CSI		WLS	
				Average of $t_{Peak,Up} -24, -12, +0, +12 h$		Average of $t_{Peak,Up} -24, -12, +0, +12 h$	
10	1,400,000; 33 h	0.11	1.00	0.97		0.01	
30	155,178; 27 min	0.34	1.02	0.91		0.08	
90	17,316; 12 min	5.80	1.07	0.68		0.23	

Note. All the models were run using a 3.40 GHz Intel(R) Core™ i7-3770 CPU with 32 GB of RAM. RMSE, root-mean-square error; PR, flood peak ratio; CSI, critical success index; WLS, water level score; G1, G2, G3, and G4, gauge locations shown in Figure 1d; $t_{Peak,Up}$, flood peak time at the upstream boundary of the computational domain.

Table 5
Performance Metrics of Models 30-Bath, R1, R2, R3, R4, E1, and E2 as Identified in Table 3

	Gauge station	RMSE	PR	Lead time	CSI	WLS
Model 30-Bath, $n = 0.03 \text{ m}^{-1/3} \text{ s}$	G1	0.49	1.02	$t_{Peak,Up} - 24 \text{ h}$	0.90	0.16
	G2	0.41	1.02	$t_{Peak,Up} - 12 \text{ h}$	0.91	0.06
	G3	0.36	1.02	$t_{Peak,Up}$	0.91	0.05
	G4	0.10	1.00	$t_{Peak,Up} + 12 \text{ h}$	0.89	0.06
Model R1, $n = 0.03 \text{ m}^{-1/3} \text{ s}$	G1	0.49	0.99	$t_{Peak,Up} - 24 \text{ h}$	0.88	0.08
	G2	0.40	0.99	$t_{Peak,Up} - 12 \text{ h}$	0.88	0.04
	G3	0.27	0.98	$t_{Peak,Up}$	0.89	0.06
	G4	0.25	0.99	$t_{Peak,Up} + 12 \text{ h}$	0.88	0.16
Model R2, $n = 0.025 \text{ m}^{-1/3} \text{ s}$	G1	1.02	0.95	$t_{Peak,Up} - 24 \text{ h}$	0.88	0.12
	G2	0.94	0.94	$t_{Peak,Up} - 12 \text{ h}$	0.88	0.08
	G3	0.59	0.95	$t_{Peak,Up}$	0.89	0.09
	G4	0.39	1.06	$t_{Peak,Up} + 12 \text{ h}$	0.86	0.21
Model R3, $n = 0.03 \text{ m}^{-1/3} \text{ s}$	G1	0.36	1.01	$t_{Peak,Up} - 24 \text{ h}$	0.90	0.09
	G2	0.33	1.01	$t_{Peak,Up} - 12 \text{ h}$	0.89	0.03
	G3	0.21	1.02	$t_{Peak,Up}$	0.91	0.09
	G4	0.56	1.01	$t_{Peak,Up} + 12 \text{ h}$	0.89	0.14
Model R4, $n = \text{from } 0.015 \text{ to } 0.07 \text{ m}^{-1/3} \text{ s}$	G1	1.03–2.41	1.05–1.10	$t_{Peak,Up} - 24 \text{ h}$	0.82–0.79	0.17–0.24
	G2	1.16–1.97	1.07–1.10	$t_{Peak,Up} - 12 \text{ h}$	0.91	0.12–0.17
	G3	1.10–1.49	1.09–1.11	$t_{Peak,Up}$	0.91	0.17–0.25
	G4	1.05–1.29	1.12–1.16	$t_{Peak,Up} + 12 \text{ h}$	0.89	0.21–0.30
Model E1, $n = 0.03 \text{ m}^{-1/3} \text{ s}$	G1	0.17	1.01	$t_{Peak,Up} - 24 \text{ h}$	0.88	0.09
	G2	0.20	1.01	$t_{Peak,Up} - 12 \text{ h}$	0.88	0.06
	G3	0.32	1.01	$t_{Peak,Up}$	0.89	0.10
	G4	0.30	0.99	$t_{Peak,Up} + 12 \text{ h}$	0.87	0.10
Model E2, $n = 0.03 \text{ m}^{-1/3} \text{ s}$	G1	0.70	1.03	$t_{Peak,Up} - 24 \text{ h}$	0.87	0.14
	G2	0.73	1.03	$t_{Peak,Up} - 12 \text{ h}$	0.87	0.11
	G3	0.90	1.05	$t_{Peak,Up}$	0.88	0.15
	G4	0.81	1.10	$t_{Peak,Up} + 12 \text{ h}$	0.86	0.16

Note. RMSE, root-mean-square error; PR, flood peak ratio; CSI, critical success index; WLS, water level score; n , Manning’s roughness coefficient; G1, G2, G3, and G4, gauge locations shown in Figure 1d; $t_{Peak,Up}$, flood peak time at the upstream boundary of the computational domain.

drives flow area variability and a uniform river bed slope could be used for flood forecast. Nevertheless, the extremely limited sensitivity of model R4 to the tested range of river roughness values underlined the importance of an adequate representation of river cross-section geometrical variability within this formulation of LISFLOOD-FP, where river geometry is discretized using a number of grid cells. Table 5 shows that a large interval of roughness values (specifically, from 0.015 to 0.07 $\text{m}^{-1/3} \text{ s}$) resulted in similarly poor R4 model performances (1.09–1.79 m average RMSE) and, differently from models R1, R2, R3, E1, and E2, a best performing roughness value could not be identified. As can be inferred from equation (3), for high values of flow depth d and discharge q , even large variations of the roughness coefficient n might have a negligible impact. For large flood events in channels wider than the computational grid size, implementations based on a prismatic channel (model R4) hamper the use of the roughness coefficient as an effective calibration parameter. Conversely, channel deepening or widening due to cross-sections depth and/or width variability in models R1, R2, and R3 led to variability in river flow depth d that enhanced the model output sensitivity to Manning’s roughness value. This analysis highlighted model R3 as a cost-effective solution when RS-derived river width values are available, and river depth can be assessed at the reach scale.

Conversely, when RS-derived river width values are not available, the results of models E1 and E2 at the point scale (E1: 0.25 m average RMSE, 1.01 average PR; E2: 0.78 m average RMSE, 1.06 average PR) and at the distributed scale (E1: 0.88 average CSI, 0.09 average WLS; E2: 0.87 average CSI, 0.14 average WLS) demonstrated that an exponential shape could represent an alternative implementation option. In contrast to the results of model R4, an exponential shape could also be advised in river reaches having limited width variability, to enhance model output sensitivity to Manning’s roughness value. Model E2 used a deep and narrow channel and its performance at the local scale was very sensitive to variations in roughness values. Moreover, its overall performance was lower than E1 showing that an accurate selection of the channel

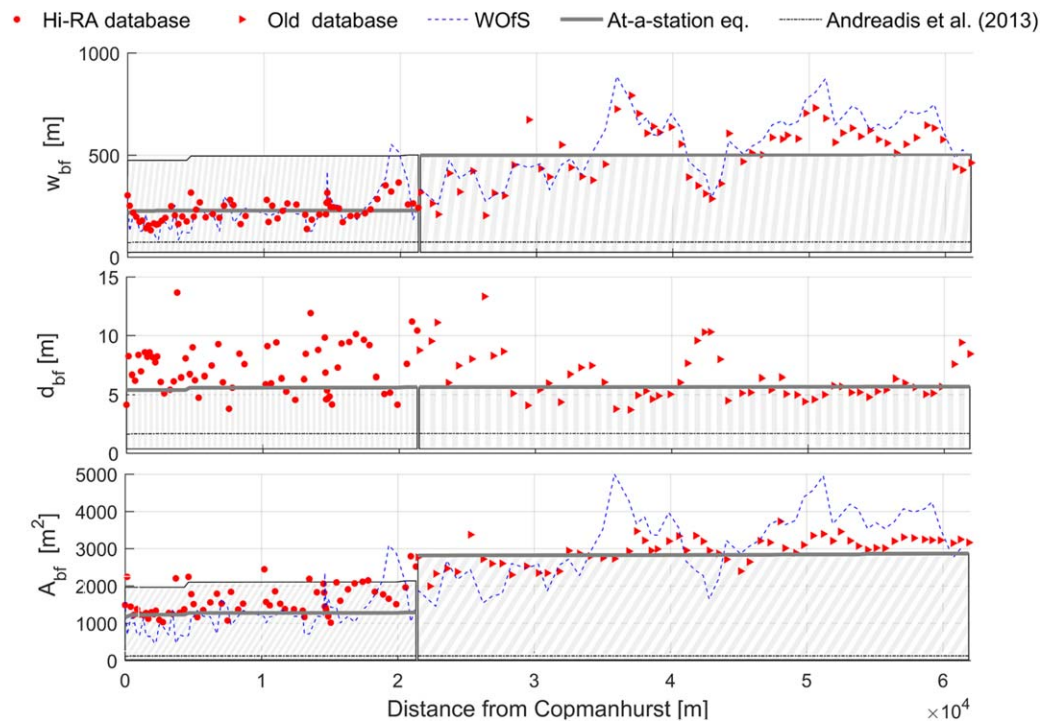


Figure 4. Comparison between field data, the RS-derived database, and the at-a-station equations as identified in Table 2. The grey striped area represents the interval of values predicted by the at-a-station equations.

shape coefficient is critical to flood modeling. Use of median value of shape coefficients derived from sampled cross sections (model E1) was a viable solution in this data-rich scenario, but care has to be taken in data-scarce scenario to avoid both near-rectangular (model R4) and near-triangular (model E2) cross sections. For this reason, the symbol E hereafter indicates an exponential cross section. Practical advice on the choice of the shape coefficient is provided in section 7.

6.2. Comparison Between Measured and Readily Available Bankfull Parameters

Figure 4 shows a comparison between measured and estimated bankfull parameters. At-a-station equations generally underestimated measured data. As shown in Table 6, global mean parameters by Andreadis et al.

Table 6
Comparison Between Field Data, RS-Derived Database, and At-A-Station Formulations

Database	RSR		PBIAS	
	Hi-RA	Old	Hi-RA	Old
(a) Bankfull width, w_{bf}				
Andreadis et al. (2013): mean value	3.03	3.22	-67.07	-85.33
Gordon (1996), Moody and Troutman (2002), and Stewardson (2005)	0.99	0.99	1.38	-1.06
WOfS, Mueller et al. (2016)	1.22	0.61	-3.21	9.88
(b) Bankfull depth, d_{bf}				
Andreadis et al. (2013): mean value	5.96	2.55	-77.12	-73.87
Gordon (1996) and De Rose et al. (2008)	1.29	1.06	-23.65	-11.58
(c) Bankfull flow area, A_{bf}				
Andreadis et al. (2013): mean value	3.76	7.79	-92.33	-95.79
Gordon (1996), Moody and Troutman (2002), Stewardson (2005), and De Rose et al. (2008)	1.47	2.41	28.94	-27.27
WOfS, Mueller et al. (2016) and De Rose et al. (2008)	1.83	1.90	-24.54	-40.0

Note. RSR, ratio of the root-mean-square error to the standard deviation of measured data; PBIAS, percent bias.

Table 7
Preliminary Assessment of the Bankfull Parameters in Data-Scarce Scenarios S1, S2, and S3

Data set	s	w_{bf}				d_{bf}				A_{bf}			
		RSR		PBIAS		RSR		PBIAS		RSR		PBIAS	
		R3	E	R3	E	R3	E	R3	E	R3	E	R3	E
S1, S2	2.6	1.22	5.11	-3.21	117.87	1.29	1.75	-23.65	-41.85	1.83	2.87	-24.54	67.93
S3	2	1.22	5.11	-3.21	117.87	2.82	1.29	-76.56	-23.65	3.19	1.47	-76.86	28.94

Note. w_{bf} , bankfull width; d_{bf} , bankfull depth; A_{bf} , bankfull flow area; s, shape coefficient; RSR, ratio of the root-mean-square error to the standard deviation of measured data; PBIAS, percent bias; R3 and E, models as defined in Table 3.

(2013) lead to a PBIAS of -67%, -77%, and -92% for the values of bankfull width, depth, and flow area of the Hi-RA database, and to a PBIAS of -85%, -74%, and -96% for the for the values of bankfull width, depth, and flow area of the Old database. For this study site, the empirical formulations derived by Gordon (1996) and the formulation of Stewardson (2005) and De Rose et al. (2008) yielded a more accurate assessment of bankfull parameters: PBIAS for width values were as low as 1% and -1% for the Hi-RA and the Old database, respectively. However, underestimation of river depth persisted with PBIAS of -24% and -12% thus leading to a PBIAS of 29% and -27% for flow area values. RS-derived width values from the WOfS database (Mueller et al., 2016) provided the most accurate representation of field data values and variability.

As shown above, selecting the most appropriate empirical formulation might be critical. A very simple approach was used here to test the benefit of integrating these readily available estimates with a limited number of field measurements. A parameterization of the at-a-station equations was selected based on input data set S1, S2, and S3 and then used to provide a preliminary assessment of the geometrical characteristics of the river reach from Copmanhurst to Mountain View. Table 7 shows the RSR and PBIAS values for the “unknown” river reach. When RS-derived width values are available, the use of empirical formulations is limited to the assessment of river depth. In this study site, as shown in Figure 4, at-a-station equations underestimated measured bankfull depth and both the data-rich S1 data set and the strategic S2 data set yielded the selection of the same parameterization of the at-a-station equations. For this reason, scenarios S1 and S2 are hereafter grouped hereafter. Specifically, in S1 and in S2, the assessment of river depth and, as a consequence, flow area was affected by a PBIAS of -24%. In scenario S3, a large underestimation of the bankfull depth (PBIAS = -77%) led to an equally large underestimation of flow area with a PBIAS as low as -77%. Conversely, within the hypothesis of nonavailability of RS-derived width values, the empirical formulations that minimize the errors in the assessment of the flow area must be used. Consequently to the morphological variability highlighted in section 4.1, in situ equations yielded a large overestimation of the river width with a PBIAS of +118%, regardless of the input data set. The use of data sets S1 and S2 yielded a large underestimation of bankfull depth with PBIAS of -42%. By chance, S3 provided more accurate estimates with a PBIAS of -24%. Errors in width and depth assessment partially compensated each other and the assessment of flow area was affected by a PBIAS of +68% for S1 and S2, and of +29% for S3. The shape coefficient was the median of the values retrieved for the sampled cross sections in S1 and S2; a parabolic cross section with $s=2$ was used in S3.

In this study site, width variability drives flow area variability and at-a-station equations generally underestimated real river depth. RS-derived width combined with a few cross sections measured at strategic locations provided a cost-effective preliminary assessment of river reach geometrical features. The use of “at-a-station” equations selected based on a few field measurements has the potential to provide information on the morphological variability of bankfull parameters at the larger scale. These equations link bankfull parameters of a river reach to the contributing catchment area. Consequently, they have the potential to provide a more physically based assessment compared to simple extrapolation of field data.

6.3. Simplified Geometries in Data-Scarce Scenarios

The model implementation in data-scarce scenarios was based on geometries R3 and E (section 6.1). Bankfull parameters were assessed based on data sets S1, S2, and S3 (section 6.2). Table 8 lists the values of the

Table 8
Performance Metrics of Models R3-S1/S2, R3-S3, E-S1/S2, and E-S3 as Identified in Table 3

	Gauge station	RMSE	PR	Lead time	CSI	WLS
MODEL R3-S1/S2, $n = 0.03 \text{ m}^{-1/3} \text{ s}$	G1	0.68	1.01	$t_{Peak,Up} - 24 \text{ h}$	0.83	0.12
	G2	0.54	1.00	$t_{Peak,Up} - 12 \text{ h}$	0.88	0.04
	G3	0.62	1.00	$t_{Peak,Up}$	0.90	0.07
	G4	0.86	1.03	$t_{Peak,Up} + 12 \text{ h}$	0.88	0.16
MODEL R3-S3, $n = 0.01 \text{ m}^{-1/3} \text{ s}$	G1	3.1	1.07	$t_{Peak,Up} - 24 \text{ h}$	0.76	0.35
	G2	2.9	1.07	$t_{Peak,Up} - 12 \text{ h}$	0.84	0.16
	G3	2.9	1.05	$t_{Peak,Up}$	0.86	0.14
	G4	1.6	0.87	$t_{Peak,Up} + 12 \text{ h}$	0.85	0.29
MODEL E-S1/S2, $n = 0.05 \text{ m}^{-1/3} \text{ s}$	G1	1.32	0.95	$t_{Peak,Up} - 24 \text{ h}$	0.66	0.27
	G2	0.78	0.98	$t_{Peak,Up} - 12 \text{ h}$	0.74	0.14
	G3	1.22	1.03	$t_{Peak,Up}$	0.78	0.17
	G4	2.39	1.25	$t_{Peak,Up} + 12 \text{ h}$	0.73	0.17
MODEL E-S3, $n = 0.055 \text{ m}^{-1/3} \text{ s}$	G1	1.31	0.97	$t_{Peak,Up} - 24 \text{ h}$	0.67	0.16
	G2	0.84	0.99	$t_{Peak,Up} - 12 \text{ h}$	0.76	0.10
	G3	0.62	1.02	$t_{Peak,Up}$	0.80	0.15
	G4	1.41	1.16	$t_{Peak,Up} + 12 \text{ h}$	0.76	0.24

Note. RMSE, root-mean-square error; PR, flood peak ratio; CSI, critical success index; WLS, water level score; n , Manning's roughness coefficient; G1, G2, G3, and G4, gauge locations shown in Figure 1d; $t_{Peak,Up}$, flood peak time at the upstream boundary of the computational domain.

performance metrics for each model setup. Information on the errors in the representation of real river geometry could be correlated to model results to assess the impact of these reach-scale approximations on flood inundation predictions. In particular, as shown in Table 7, R3-S1/S2 and R3-S3 slightly (PBIAS = -25%) and largely (PBIAS = -77%) underestimated bankfull flow area at the reach scale; E-S3 and E-S1/S2 moderately (PBIAS = +29%) and largely (PBIAS = +68%) overestimated bankfull flow area at the reach scale.

Model R3-S1/S2 was able to reproduce the high-resolution benchmark model with similar performance metric values as the model 30-Bath at the point scale (0.67 m average RMSE, 1.01 average PR) and at the catchment scale (0.87 average CSI, 0.10 average WLS). Conversely, models R3-S3, E-S1/S2, and E-S3 had lower performances; specifically, a unique model parameterization that allowed equally good performances at any gauge station and any lead time could not be identified. For the purpose of this sensitivity analysis, the Manning's roughness value was selected to minimize errors in the prediction of inundation extent and level 12 h before and at $t_{Peak,Up}$. This choice was motivated by the results of previous data assimilation and calibration studies which showed the effectiveness of RS images obtained during the rising limb and up to the flood peak to constrain model parameter space (e.g., Garcia-Pintado et al., 2013; Gobeyn et al., 2017).

As expected, a low value of Manning's roughness coefficient was suggested for models R3-S3, while high values of Manning's roughness coefficients were suggested for models E-S1/S2 and E-S3. Nevertheless, large variations in model performances at different gauge stations and different lead times (Table 8) suggested that, for these models, a simple tuning of the friction parameter at the reach scale could not yield accurate forecasts. Spatial or temporal variation of the roughness parameters to locally fit water levels or reduce prediction errors at different lead times was not applied here. In fact, such a solution has been discouraged by previous studies (Kirchner, 2006; Matgen et al., 2010; Neal et al., 2015).

In this numerical experiment, the artificially high number of gauge stations and synthetic RS observations clearly highlighted errors in the implementation of models R3-S3, E-S1/S2, and E-S3. However, this problem might be difficult to detect in a real case scenario, where a limited number of validation data are available. Manning's roughness coefficient is an effective parameter and deviations from physically realistic values are expected (as in R3-S3). On the contrary, as pointed out by Stephens and Bates (2015), a false sense of overconfidence in a models' robustness can derive from physically realistic values of the friction coefficient (as in E-S1/S2 and E-S3). Moreover, in the case of fast moving flood events in V-shaped valleys, fitness metrics that evaluate model performance at the catchment scale (CSI and WLS) might be difficult to interpret, as overprediction and underprediction errors can compensate for each other. Conversely, this study showed that the comparison of modeled and benchmark water levels at the spatially distributed scale, for different

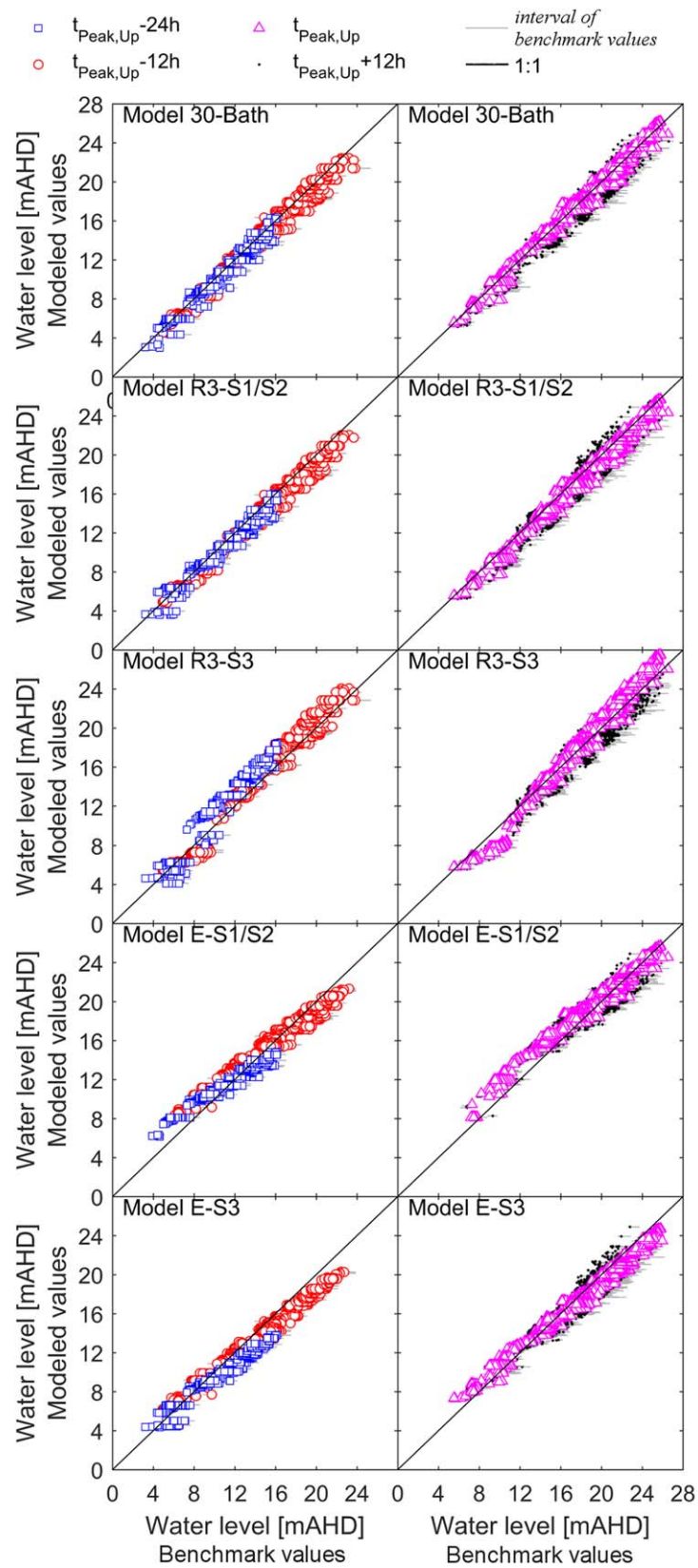


Figure 5. Comparison of models 30-Bath, R3-S1/S2, R3-S3, E-S1/S2, and E-S3 as identified in Table 3: spatial distributions of modeled and benchmark water levels at different times, including rising (left column) and falling (right column) limbs.

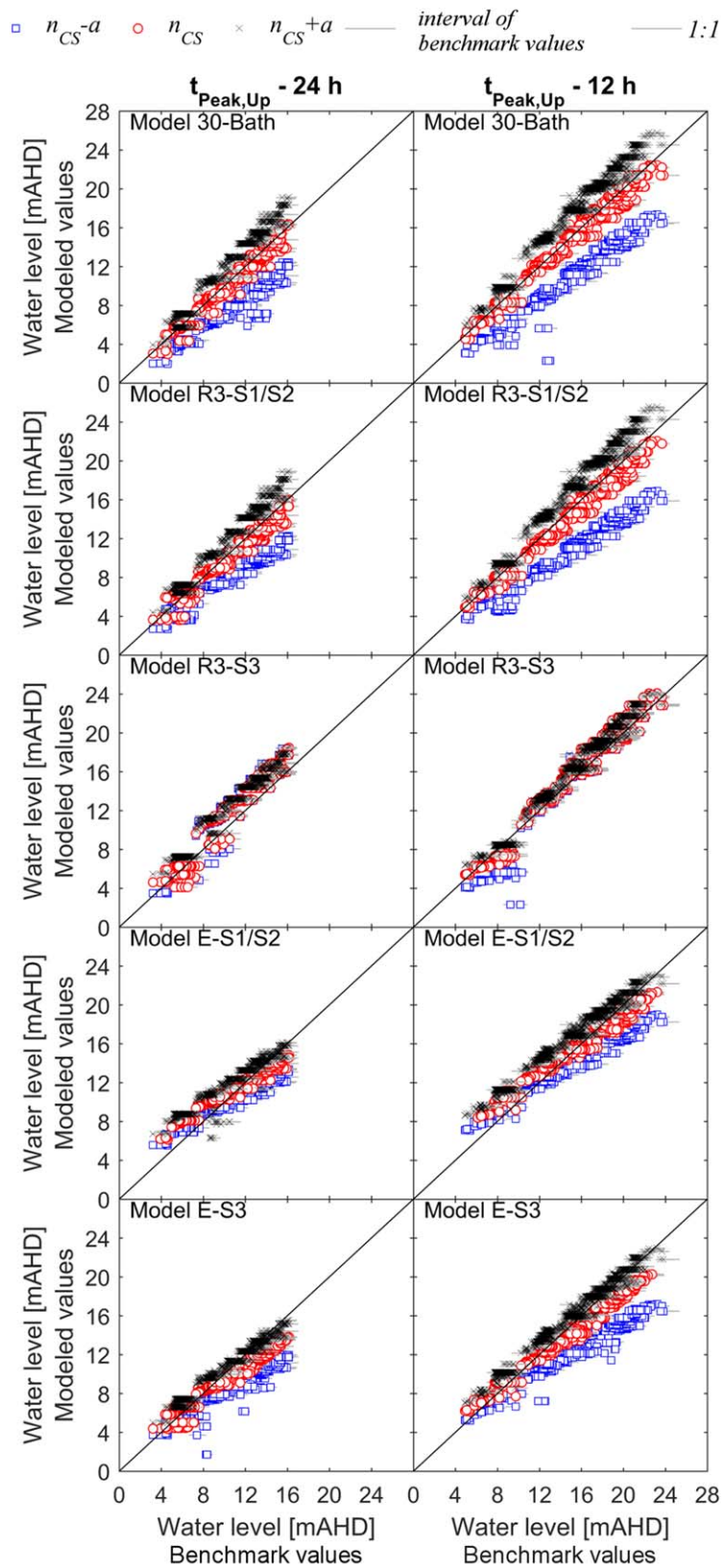


Figure 6. Comparison of models 30-Bath, R3-S1/S2, R3-S3, E-S/S2, and E-S3 as identified in Table 3: modeled and benchmark water levels at (left column) $t_{Peak,Up} - 24 \text{ h}$ and (right column) $t_{Peak,Up} - 12 \text{ h}$ for different values of river roughness coefficients ($a = 0.005 \text{ m}^{-1/3} \text{ s}$ for R3-S3; $a = 0.01 \text{ m}^{-1/3} \text{ s}$ elsewhere).

lead times (Figures 5 and 6), allowed a more thorough understanding of the relative impacts of river geometry and roughness on flood dynamics.

In model R3-S1/S2 (Figure 5), modeled and benchmark water levels aligned with the 1:1 line at any time slice. This behaviour was consistent with the model 30-Bath (Figure 5). In fact, model R3-S1/S2 slightly underestimated benchmark water levels. Nevertheless, the consistency of this discrepancy at the catchment scale suggested that a finer tuning of the roughness coefficient had the potential to improve the performance of model R3-S1/S2. In model R3-S3, the selected low value of river roughness partially compensated for the underestimation of flow capacity and limited the overestimation of benchmark water levels in the upstream area of the catchment. However, this parameterization led to underestimation of the benchmark water level in the downstream area of the catchment. This analysis is confirmed by peak ratio values considerably higher than 1 for G1, G2, and G3 and considerably lower than 1 for G4 (Table 8). It is worth noting that the analysis of spatially distributed water levels at any of the selected lead times yielded the same conclusion inferred from an artificially dense gauge stations network. In models E-S1/S2 and E-S3, a high friction coefficient was used to compensate for the overestimation of river flow capacity at the catchment scale. This parametrization resulted in underestimation of benchmark water levels in the upstream area of the catchment and overestimation of benchmark water levels in the downstream area of the catchment as shown in Figure 5. These results are confirmed by the analysis of the peak ratio values (Table 8). Similar to model R3-S3, a dense gauge network was required to highlight errors in model implementation. Conversely, a similar diagnosis could be inferred from the analysis of the spatial pattern of distributed water levels at any of the selected lead times.

The qualitative description above has been quantified by a simple linear fitting of the values of modeled and true water levels by

$$\text{Water level, modeled values} = I_1 \cdot \text{Water level, benchmark values} + I_2, \tag{7}$$

where I_1 and I_2 are the coefficients of the linear regression. The results of this simple linear fitting are reported in Table 9. The coefficient I_1 is close to 1 for models 30-Bath and R3-S1/S2; higher than 1 for model R3-S3; and lower than 1 for models E-S1/S2 and E-S3.

The analysis above suggested that, despite models R3-S1/S2 and E-S3 being affected by similar absolute errors in the assessment of flow capacity at the catchment scale, model R3-S1/S2 allowed for a more realistic representation of inundation dynamics. In this study site, where variations in river width are relevant (section 6.2), RS-derived river width values provided an effective surrogate representation of geometric channel variability which proved to be relevant for the modeling of flood inundation dynamics. Furthermore, in model R3-S1/S2, width variability acted as geometrical roughness that partially compensated for the overestimation of the real flow capacity at the reach scale.

The next paragraph shows how a simple analysis of the spatial distribution of modeled and benchmark water levels and of their sensitivity to small variation of river roughness could provide an effective strategy for the detection of inappropriate geometrical representations of river bathymetry. In this study site, this diagnosis was successful even at the very early stages of the flood event; that is, as early as 24 h before the

Table 9
Values of Coefficients I_1 and I_2 of the Linear Regression of Modeled and Benchmark Inundation Level at Different Lead Times

Lead time	Model									
	30-Bath		R3-S1/S2		R3-S3		E-S1/S2		E-S3	
	I_1	I_2	I_1	I_2	I_1	I_2	I_1	I_2	I_1	I_2
$t_{Peak,Up} - 24$ h	0.95	0.27	0.90	0.88	1.19	-0.55	0.65	4.30	0.71	2.26
$t_{Peak,Up} - 12$ h	0.98	0.14	0.95	0.16	1.18	-2.14	0.75	4.13	0.77	2.62
$t_{Peak,Up}$	0.99	0.15	0.98	-0.20	1.20	-3.47	0.83	3.80	0.84	2.46
$t_{Peak,Up} + 12$ h	0.99	-0.30	0.95	-0.23	1.14	-3.01	0.76	4.68	0.80	2.85

Note. $t_{Peak,Up}$ flood peak time at the upstream boundary of the computational domain. Models 30-Bath, R3-S1/S2, R3-S3, E-S1/S2, and E-S3 as identified in Tables 3 and 7.

Table 10
 Values of Coefficients l_1 and l_2 of the Linear Regression of Modeled and Benchmark Inundation Level at Different Lead Times for Different Values of the River Roughness Coefficient

Lead time	Roughness coefficient	Model									
		30-Bath		R3-S1/S2		R3-S3		E-S1/S2		E-S3	
		l_1	l_2	l_1	l_2	l_1	l_2	l_1	l_2	l_1	l_2
$t_{Peak,Up} - 24$ h	$n_{CS} - a$	0.71	-0.06	0.67	1.03	1.33	-2.29	0.59	3.79	0.61	2.02
	n_{CS}	0.95	0.27	0.90	0.88	1.19	-0.55	0.65	4.30	0.71	2.26
	$n_{CS} + a$	1.14	0.21	1.09	0.70	1.06	1.29	0.71	4.51	0.79	2.59
$t_{Peak,Up} - 12$ h	$n_{CS} - a$	0.77	-0.51	0.70	0.38	1.32	-4.61	0.66	3.87	0.64	2.49
	n_{CS}	0.98	0.14	0.95	0.16	1.18	-2.14	0.75	4.13	0.77	2.62
	$n_{CS} + a$	1.11	0.76	1.11	0.24	1.09	-0.43	0.83	4.34	0.88	2.79

Note. n_{CS} , Manning's roughness parameter suggested by the analysis of the performance metrics at the catchment scale. $a = 0.005 \text{ m}^{-1/3} \text{ s}$ for R3-S3; $a = 0.01 \text{ m}^{-1/3} \text{ s}$ elsewhere. $t_{Peak,Up}$, flood peak time at the upstream boundary of the computational domain. Models 30-Bath, R3-S1/S2, R3-S3, E-S1/S2, and E-S3 as identified in Tables 3 and 7.

flood peak at the input point of the computational domain. Figure 6 shows the spatial distribution of modeled and benchmark water levels at $t_{Peak,Up} - 24$ h and at $t_{Peak,Up} - 12$ h for models 30-Bath, R3-S1/S2, R3-S1/S2, and R3-S3. For each model implementation, the graph shows the results for the Manning's roughness value selected based on the analysis at the catchment scale (n_{CS} , Tables 7 and 8) and when each of these selected values was decreased or increased by $0.01 \text{ m}^{-1/3} \text{ s}$ (with the exception of model R3-S3, for which the increment was $0.005 \text{ m}^{-1/3} \text{ s}$). Table 10 lists the coefficients of the linear regression of modeled and benchmark water levels for each model realisation of Figure 6. In robust model implementations, such as 30-Bath and R3-S1/S2, modeled and benchmark water levels aligned along the 1:1 line for the Manning's value selected from the analysis of the performance metrics evaluated at the catchment scale (i.e., RMSE, PR, CSI, and WLS). Conversely, when lower or higher Manning's roughness values were used, the models consistently underestimated or overestimated the benchmark water levels. For these model simulations, all the points in Figure 6 were either below or above the 1:1 line (the discrepancy was less evident downstream because of the impact of the tidal boundary conditions), and the slope coefficient l_1 was either lower or higher than 1 (Table 10). These results were consistent at the two selected lead times. The patterns of the spatial distribution of modeled and benchmark water levels for model R3-S3 were quite different. When the Manning's roughness parameter suggested by the analysis of the performance metrics at the catchment scale was adopted, modeled water levels overestimated benchmark water level values upstream and underestimated benchmark water level values downstream. Upstream overestimation and downstream underestimation decreased and increased for lower values of Manning's roughness coefficient, while increased and decreased for higher values of Manning's roughness coefficient. As a consequence, the points in Figure 6 were distributed around a fictitious line having a slope higher than 1, as confirmed by the l_1 values in Table 10. Conversely, for model simulations based on geometry E-S1/S2 and E-S3, the points in Figure 6 were distributed around a fictitious line having a lower slope than the 1:1 line as shown by the l_1 values in Table 10.

7. Conclusions and Future Work

Knowledge on river bathymetry is essential to simulate floodplain inundation. River depth and shape cannot be systematically observed remotely and field data are expensive and extremely rare. A parsimonious methodology is needed for the definition of effective river bathymetry to support the implementation of operational flood forecasting hydraulic models. In this paper, a detailed field database and a numerical experiment were used to (i) investigate which simplified geometries allowed sufficient physical representation of inundation dynamics; (ii) outline a methodology for the preliminary off-line assessment of river geometry; and (iii) suggest a strategy to detect errors in this preliminary assessment.

The hydraulic model LISFLOOD-FP was used to simulate a hypothetical flood event in a meandering reach of the Clarence River (Australia), for which detailed bathymetric data were available. A high-resolution model simulation based on this detailed bathymetric data set was considered as the benchmark for ranking the performances of a number of coarser model realizations in which the channel was represented using

simplified geometries derived from a combination of field data, global database, and RS data. Using this study site as a test-case, a methodology was developed for parsimonious representation of geometrical variability with inundation extent and level found to be more sensitive to river bathymetry than roughness.

The first outcome of this study was identification of a rectangular, width-varying shape with uniform longitudinal slope as the most effective simplified geometrical model. Second, a methodology for the preliminary assessment of river geometry was outlined. Specifically, for the implementation of a rectangular, width-varying shape, width values can be derived from RS data while depth values can be assessed using a combination of global databases and limited field data. Where RS-derived width data are not available or show negligible reach variability, an exponential cross-section shape was recommended. In this latter scenario, shape, depth and width were estimated based on a thorough comparison between limited field data, remote sensing data and at-a-station equations. Field data collection is limited to the measurement of river cross sections at a minimum of three locations evenly distributed along the river reach under investigation. Where measurements of the study reach are not feasible, exploration of a similar length of the adjoining river reach is advised. Measured river cross sections should have different width, and, when applicable, should be located in the proximity of geomorphologic features (such as restrictions and widenings as identified by a visual analysis of Google Earth). Median or mean shape coefficient values are advised. A parabolic shape could represent a viable solution to avoid near-rectangular and near-triangular cross sections. Such a preliminary assessment of river geometry has the potential to reduce the uncertainty of an ill-posed problem and support RS-based data assimilation or calibration studies, as advocated by many previous studies (e.g., Durand et al., 2014; Garambois & Monnier, 2015; García-Pintado et al., 2015).

A number of data-scarce scenarios were hypothesized to investigate the effects of errors in the representation of river geometry and flow capacity on inundation dynamics. The third outcome of this study is the demonstration that the analysis of the discrepancy between modeled and benchmark water levels at the full catchment scale revealed errors in the model implementation. Specifically, distributed water levels derived from a synthetic RS observation acquired as early as 24 h before the flood peak at the input point of a short river reach was useful to diagnose errors in the model implementation. In a real case study, such a comparison could be used to complement the information on model accuracy provided by lumped performance metrics such as the *WLS* (Savage et al., 2016a), the Student's *t* test (Mason et al., 2009), and the RMSE (Stephens et al., 2012).

In the implementation of LISFLOOD-FP used in this study, river bathymetry is discretised using a number of cells. A subgrid version of LISFLOOD-FP has been developed (Neal et al., 2012, 2015) for flood modeling at continental to global scale, where a computational grid size larger than river width has to be used (e.g., Schumann et al., 2015). Its application at the smaller scale of operational flood forecasting systems should be coupled with algorithms designed to downscale coarse model outputs to the desired resolution (e.g., Schumann et al., 2014). The fine-scale analysis developed in this study could be useful to benchmark subgrid model realizations where channel flow is modeled using a specific routine. In this specific routine, the use of analytical equations to compute channel wetted area and perimeter enhances the sensitivity of prismatic channel geometry to roughness values. Along with the possibility of using a prismatic channel within the subgrid modeling framework, it would be interesting to test the considerations on surface roughness and geometrical roughness developed in this case study.

Clearly, there are limitations to extrapolating the findings of this study to other flood events and other catchments and further testing to explore the relevance of flood magnitude and the relative importance of river incision, width variability and sinuosity is required. Moreover, in the numerical experiment discussed here, river bathymetry was the only source of uncertainty. In a real case scenario, both epistemic uncertainties (attributable to the imperfect knowledge of the processes) and aleatory uncertainties (resulting from the randomness of systems and processes) should be taken into account (Beven & Freer, 2001).

This study aimed to shed light on the complex patterns and dependencies between river bathymetry, roughness, and inundation dynamics. The importance of structural correction provided by an adequate representation of channel geometric variability and the potential benefit of acquiring satellite images at the early stages of a flood event were highlighted by this numerical experiment. Specifically, this numerical experiment showed the potential informative value of comparing patterns of modeled and RS-derived spatially distributed water levels. However, in a real case scenario, the impact of uncertainties in RS-derived

observations on the use of this data for the diagnosis of errors in model implementation and thus improve floodplain forecasting skill has to be carefully evaluated. Finally, the existence of epistemic and aleatory uncertainties clearly imply that models should not point out a singular “best performing” simulation but multiple acceptable models for the provision of possibility of inundation maps (e.g., Aronica et al., 2002; Neal et al., 2013; Savage et al., 2016a)

Acknowledgments

This project was funded through the Bushfire and Natural Hazards Collaborative Research Centre grant “Improving flood forecast skill using remote sensing data,” and through the Monash Faculty of Engineering seed grants “Optimization of a hydraulic model using a Doppler profiler” and “Strategic high-resolution monitoring of streams to improve operational flood forecasts.” Valentijn Pauwels is funded through the Australian Research Council Future Fellowship grant FT130100545. The authors express their gratitude to the Clarence Valley Council, BMT-WBM Ltd, the Australian Bureau of Meteorology, Geoscience Australia, and the Commonwealth Scientific and Industrial Research Organisation for their advice and support during the collection of the remote sensing and field database. The authors thank Ben O’Connor, the two anonymous reviewers, and the Associate Editor who provided comments that helped improve the quality of the manuscript. Gauge station 204007 is maintained by the Australian Bureau of Meteorology (<http://www.bom.gov.au/waterdata/>); gauge station 204414 is maintained by New South Wales Manly Hydraulics Laboratory (<http://new.mhl.nsw.gov.au/Site-204414>). The copyright of the 1 m Lidar Digital Elevation Model (DEM) is owned by New South Wales Land and Property Management Authority (<https://six.nsw.gov.au/>; <http://elevation.fsdf.org.au/>). The Old bathymetric database is available for noncommercial purposes by contacting the Clarence Valley Council (council@clarence.nsw.gov.au). The Hi-RA bathymetric database is available from <https://figshare.com/s/734013570be9aecbf8ba> (<https://doi.org/10.4225/03/5a20708405ecd>).

References

- Alfieri, L., Feyen, L., Salamon, P., Thielen, J., Bianchi, A., Dottori, F., et al. (2016). Modelling the socio-economic impact of river floods in Europe. *Natural Hazards and Earth System Sciences*, 16(6), 1401–1411. <https://doi.org/10.5194/nhess-16-1401-2016>
- Allen, G. H., & Pavelsky, T. M. (2015). Patterns of river width and surface area revealed by the satellite-derived North American River Width data set. *Geophysical Research Letters*, 42, 395–402. <https://doi.org/10.1002/2014GL02764>
- Alsdorf, D., Bates, P., Melack, J., Wilson, M., & Dunne, T. (2007a). Spatial and temporal complexity of the Amazon flood measured from space. *Geophysical Research Letters*, 34, L08402. <https://doi.org/10.1029/2007GL029447>
- Alsdorf, D. E., Rodríguez, E., & Lettenmaier, D. P. (2007b). Measuring surface water from space. *Reviews of Geophysics*, 45, RG2002. <https://doi.org/10.1029/2006RG000197>
- Altenau, E. H., Pavelsky, T. M., Bates, P. D., & Neal, J. C. (2017). The effects of spatial resolution and dimensionality on modeling regional-scale hydraulics in a multichannel river. *Water Resources Research*, 53, 1683–1701. <https://doi.org/10.1002/2016WR019396>
- Andreadis, K. M., Clark, E. A., Lettenmaier, D. P., & Alsdorf, D. E. (2007). Prospects for river discharge and depth estimation through assimilation of swath-altimetry into a raster-based hydrodynamics model. *Geophysical Research Letters*, 34, L10403. <https://doi.org/10.1029/2007GL029721>
- Andreadis, K. M., Schumann, G. J. P., & Pavelsky, T. (2013). A simple global river bankfull width and depth database. *Water Resources Research*, 49, 7164–7168. <https://doi.org/10.1002/wrcr.20440>
- Aronica, G., Bates, P. D., & Horritt, M. S. (2002). Assessing the uncertainty in distributed model predictions using observed binary pattern information within GLUE. *Hydrological Processes*, 16(10), 2001–2016. <https://doi.org/10.1002/hyp.398>
- Bates, P. D., & De Roo, A. P. J. (2000). A simple raster-based model for flood inundation simulation. *Journal of Hydrology*, 236(1–2), 54–77. [https://doi.org/10.1016/S0022-1694\(00\)00278-X](https://doi.org/10.1016/S0022-1694(00)00278-X)
- Bates, P. D., Horritt, M. S., & Fewtrell, T. J. (2010). A simple inertial formulation of the shallow water equations for efficient two-dimensional flood inundation modelling. *Journal of Hydrology*, 387(1–2), 33–45. <https://doi.org/10.1016/j.jhydrol.2010.03.027>
- Bates, P. D., Horritt, M. S., Smith, C. N., & Mason, D. (1997). Integrating remote sensing observations of flood hydrology and hydraulic modelling. *Hydrological Processes*, 11(14), 1777–1795. [https://doi.org/10.1002/\(SICI\)1099-1085\(199711\)11:14<1777::AID-HYP543>3.0.CO;2-E](https://doi.org/10.1002/(SICI)1099-1085(199711)11:14<1777::AID-HYP543>3.0.CO;2-E)
- Beven, K., & Freer, J. (2001). Equifinality, data assimilation, and uncertainty estimation in mechanistic modelling of complex environmental systems using the GLUE methodology. *Journal of Hydrology*, 249(1–4), 11–29. [https://doi.org/10.1016/S0022-1694\(01\)00421-8](https://doi.org/10.1016/S0022-1694(01)00421-8)
- Biancamaria, S., Andreadis, K. M., Durand, M., Clark, E. A., Rodriguez, E., Mognard, N. M., et al. (2010). Preliminary characterization of SWOT hydrology error budget and global capabilities. *IEEE Journal of Selected Topics in Applied Earth Observations and Remote Sensing*, 3(1), 6–19. <https://doi.org/10.1109/JSTARS.2009.2034614>
- Biancamaria, S., Lettenmaier, D. P., & Pavelsky, T. M. (2016). The SWOT mission and its capabilities for land hydrology. *Surveys in Geophysics*, 37, 307–337. <https://doi.org/10.1007/s10712-015-9346-y>
- Buffington, J. M. (2012). *Changes in channel morphology over human time scales gravel-bed rivers* (pp. 433–463). Hoboken, NJ: John Wiley.
- Camporese, M., Paniconi, C., Putti, M., & Orlandini, S. (2010). Surface-subsurface flow modeling with path-based runoff routing, boundary condition-based coupling, and assimilation of multisource observation data. *Water Resources Research*, 46, W02512. <https://doi.org/10.1029/2008WR007536>
- Castellarin, A., Di Baldassarre, G., Bates, P. D., & Brath, A. (2009). Optimal cross-sectional spacing in Preissmann scheme 1D hydrodynamic models. *Journal of Hydraulic Engineering*, 135(2), [https://doi.org/10.1061/\(ASCE\)0733-9429\(2009\)135:2\(96](https://doi.org/10.1061/(ASCE)0733-9429(2009)135:2(96)
- Chow, V. (1959). *Open-channel hydraulics*. New York, NY: McGraw-Hill.
- Conner, J. T., & Tonina, D. (2014). Effect of cross-section interpolated bathymetry on 2D hydrodynamic model results in a large river. *Earth Surface Processes and Landforms*, 39(4), 463–475. <https://doi.org/10.1002/esp.3458>
- CRED, & UNISDR. (2015). *The human cost of weather-related disasters 1995–2015*. Retrieved from <https://www.unisdr.org/we/inform/publications/46796>
- Cunge, J. A., Holly, F. M., & Verwey, A. (1980). *Practical aspects of computational river hydraulics*. Boston, MA: Pitman.
- de Almeida, G. A. M., Bates, P., Freer, J. E., & Souvignet, M. (2012). Improving the stability of a simple formulation of the shallow water equations for 2-D flood modeling. *Water Resources Research*, 48, W05528. <https://doi.org/10.1029/2011WR011570>
- De Groeve, T., Thielen-del Pozo, J., Brakenridge, R., Adler, R., Alfieri, L., Kull, D., et al. (2015). Joining forces in a global flood partnership. *Bulletin of the American Meteorological Society*, 96(5), 1–4. <https://doi.org/10.1175/BAMS-D-14-00147.1>
- De Rose, R. C., Stewardson, M. J., & Harman, C. (2008). Downstream hydraulic geometry of rivers in Victoria, Australia. *Geomorphology*, 99(1), 302–316. <https://doi.org/10.1016/j.geomorph.2007.11.008>
- Dewelde, J., Verbeke, S., Quintelier, E., Cabus, P., Vermeulen, A., Vansteenkiste, T., et al. (2014). *Real-time flood forecasting systems in Flanders*. Paper presented at the 11th International Conference on Hydroinformatics, New York, USA, August 17–21 2014.
- Dingman, L. S. (2007). Analytical derivation of at-a-station hydraulic-geometry relations. *Journal of Hydrology*, 334(1), 17–27. <https://doi.org/10.1016/j.jhydrol.2006.09.021>
- Dingman, S. L. (2009). *Fluvial hydraulics*. Cary, NC: Oxford University Press.
- Dottori, F., Di Baldassarre, G., & Todini, E. (2013). Detailed data is welcome, but with a pinch of salt: Accuracy, precision, and uncertainty in flood inundation modeling. *Water Resources Research*, 49, 6079–6085. <https://doi.org/10.1002/wrcr.20406>
- Durand, M., Andreadis, K. M., Alsdorf, D. E., Lettenmaier, D. P., Moller, D., & Wilson, M. (2008). Estimation of bathymetric depth and slope from data assimilation of swath altimetry into a hydrodynamic model. *Geophysical Research Letters*, 35, L20401. <https://doi.org/10.1029/2008GL034150>
- Durand, M., Neal, J., Rodríguez, E., Andreadis, K. M., Smith, L. C., & Yoon, Y. (2014). Estimating reach-averaged discharge for the River Severn from measurements of river water surface elevation and slope. *Journal of Hydrology*, 511, 92–104. <https://doi.org/10.1016/j.jhydrol.2013.12.050>

- Erskine, W. D., Saynor, M. J., & Lowry, J. (2006). *Classification of Australian tropical rivers to predict climate change impacts*. Paper presented at the Proceedings 9th International Rivers Symposium, Brisbane, September 4–7 2006.
- Fewtrell, T. J., Bates, P. D., Horritt, M., & Hunter, N. M. (2008). Evaluating the effect of scale in flood inundation modelling in urban environments. *Hydrological Processes*, 22(26), 5107–5118. <https://doi.org/10.1002/hyp.7148>
- Fewtrell, T. J., Neal, J. C., Bates, P. D., & Harrison, P. J. (2011). Geometric and structural river channel complexity and the prediction of urban inundation. *Hydrological Processes*, 25(20), 3173–3186. <https://doi.org/10.1002/hyp.8035>
- Frasson, R. P. D. M., Wei, R., Durand, M., Minear, J. T., Domeneghetti, A., Schumann, G., et al. (2017). Automated river reach definition strategies: Applications for the Surface Water and Ocean Topography mission. *Water Resources Research*, 53, 8164–8186. <https://doi.org/10.1002/2017WR020887>
- Garambois, P.-A., & Monnier, J. (2015). Inference of effective river properties from remotely sensed observations of water surface. *Advances in Water Resources*, 79, 103–120. <https://doi.org/10.1016/j.advwatres.2015.02.007>
- García-Pintado, J., Mason, D. C., Dance, S. L., Cloke, H. L., Neal, J. C., Freer, J., et al. (2015). Satellite-supported flood forecasting in river networks: A real case study. *Journal of Hydrology*, 523, 706–724. <https://doi.org/10.1016/j.jhydrol.2015.01.084>
- García-Pintado, J., Neal, J. C., Mason, D. C., Dance, S. L., & Bates, P. D. (2013). Scheduling satellite-based SAR acquisition for sequential assimilation of water level observations into flood modelling. *Journal of Hydrology*, 495, 252–266. <https://doi.org/10.1016/j.jhydrol.2013.03.050>
- Giustarini, L., Hostache, R., Kavetski, D., Chini, M., Corato, G., Schläffer, S., et al. (2016). Probabilistic flood mapping using synthetic aperture radar data. *IEEE Transactions on Geoscience and Remote Sensing*, 54(12), 6958–6969. <https://doi.org/10.1109/TGRS.2016.2592951>
- Gleason, C. J., & Wang, J. (2015). Theoretical basis for at-many-stations hydraulic geometry. *Geophysical Research Letters*, 42, 7107–7114. <https://doi.org/10.1002/2015GL064935>
- Glenn, J., Tonina, D., Morehead, M. D., Fiedler, F., & Benjankar, R. (2016). Effect of transect location, transect spacing and interpolation methods on river bathymetry accuracy. *Earth Surface Processes and Landforms*, 41(9), 1185–1198. <https://doi.org/10.1002/esp.3891>
- Gobeyn, S., Van Wesemael, A., Neal, J., Lievens, H., Van Eerdenbrugh, K., De Vleeschouwer, N., et al. (2017). Impact of the timing of a SAR image acquisition on the calibration of a flood inundation model. *Advances in Water Resources*, 100, 126–138. <https://doi.org/10.1016/j.advwatres.2016.12.005>
- Gordon, N. G. (1996). *The hydraulic geometry of the Acheron River, Victoria, Australia*. Parkville VIC, Australia: University of Melbourne.
- Grimaldi, S., Li, Y., Pauwels, V. R. N., & Walker, J. P. (2016). Remote sensing-derived water extent and level to constrain hydraulic flood forecasting models: Opportunities and challenges. *Surveys in Geophysics*, 37(5), 977–1034. <https://doi.org/10.1007/s10712-016-9378-y>
- Harman, C., Stewardson, M., & DeRose, R. (2008). Variability and uncertainty in reach bankfull hydraulic geometry. *Journal of Hydrology*, 351(1), 13–25. <https://doi.org/10.1016/j.jhydrol.2007.11.015>
- Hilton, J. (2017). *GEM geospatial editor (version v1): CSIRO. Software collection*. Retrieved from <https://doi.org/10.4225/08/5a1611629ab3d>
- Horritt, M. S., & Bates, P. D. (2001). Effects of spatial resolution on a raster based model of flood flow. *Journal of Hydrology*, 253(1), 239–249. [https://doi.org/10.1016/S0022-1694\(01\)00490-5](https://doi.org/10.1016/S0022-1694(01)00490-5)
- Hostache, R., Matgen, P., Giustarini, L., Teferle, F. N., Tailliez, C., Iffly, J. F., et al. (2015). A drifting GPS buoy for retrieving effective riverbed bathymetry. *Journal of Hydrology*, 520, 397–406. <https://doi.org/10.1016/j.jhydrol.2014.11.018>
- Hunter, N. M., Bates, P. D., Horritt, M. S., & Wilson, M. D. (2007). Simple spatially-distributed models for predicting flood inundation: A review. *Geomorphology*, 90(3), 208–225. <https://doi.org/10.1016/j.geomorph.2006.10.021>
- Huxley, C., & Farr, A. (2013). *Lower Clarence flood model update 2013*. Brisbane, Australia: BMT WBM Ltd.
- Jarihani, A. A., Callow, J. N., McVicar, T. R., Van Niel, T. G., & Larsen, J. R. (2015). Satellite-derived Digital Elevation Model (DEM) selection, preparation and correction for hydrodynamic modelling in large, low-gradient and data-sparse catchments. *Journal of Hydrology*, 524, 489–506. <https://doi.org/10.1016/j.jhydrol.2015.02.049>
- Jung, H., & Jasinski, M. (2015). Sensitivity of a floodplain hydrodynamic model to satellite-based DEM scale and accuracy: Case study—The Atchafalaya Basin. *Remote Sensing*, 7(6), 7938.
- Jung, H. C., Jasinski, M., Kim, J.-W., Shum, C. K., Bates, P., Neal, J., et al. (2012). Calibration of two-dimensional floodplain modeling in the central Atchafalaya Basin Floodway System using SAR interferometry. *Water Resources Research*, 48, W07511. <https://doi.org/10.1029/2012WR011951>
- Kalyanapu, A. J., Shankar, S., Pardyjak, E. R., Judi, D. R., & Burian, S. J. (2011). Assessment of GPU computational enhancement to a 2D flood model. *Environmental Modelling & Software*, 26(8), 1009–1016. <https://doi.org/10.1016/j.envsoft.2011.02.014>
- Kinzel, P. J., Legleiter, C. J., & Nelson, J. M. (2013). Mapping river bathymetry with a small footprint green LiDAR: Applications and challenges. *JAWRA Journal of the American Water Resources Association*, 49(1), 183–204. <https://doi.org/10.1111/jawr.12008>
- Kirchner, J. W. (2006). Getting the right answers for the right reasons: Linking measurements, analyses, and models to advance the science of hydrology. *Water Resources Research*, 42, W03S04. <https://doi.org/10.1029/2005WR004362>
- Legleiter, C. J. (2015). Calibrating remotely sensed river bathymetry in the absence of field measurements: Flow REsistance Equation-Based Imaging of River Depths (FREEBIRD). *Water Resources Research*, 51, 2865–2884. <https://doi.org/10.1002/2014WR016624>
- Legleiter, C. J., Roberts, D. A., & Lawrence, R. L. (2009). Spectrally based remote sensing of river bathymetry. *Earth Surface Processes and Landforms*, 34(8), 1039–1059. <https://doi.org/10.1002/esp.1787>
- Lehner, B., & Grill, G. (2013). Global river hydrography and network routing: Baseline data and new approaches to study the world's large river systems. *Hydrological Processes*, 27(15), 2171–2186. <https://doi.org/10.1002/hyp.9740>
- Lehner, B., Verdin, K., & Jarvis, A. (2008). New global hydrography derived from spaceborne elevation data. *Eos, Transactions American Geophysical Union*, 89(10), 93–94. <https://doi.org/10.1029/2008EO100001>
- Leopold, L. B., & Maddock, T. (1953). *Hydraulic geometry of stream channels and some physiographic implications*. Washington, DC: U.S. Government Printing Office.
- Li, Y., Grimaldi, S., Walker, J., & Pauwels, V. (2016). Application of remote sensing data to constrain operational rainfall-driven flood forecasting: A review. *Remote Sensing*, 8(6), 456. <https://doi.org/10.3390/rs8060456>
- Mason, D. C., Bates, P. D., & Dall'Amico, J. T. (2009). Calibration of uncertain flood inundation models using remotely sensed water levels. *Journal of Hydrology*, 368(1–4), 224–236. <https://doi.org/10.1016/j.jhydrol.2009.02.034>
- Mason, D. C., Schumann, G. J. P., Neal, J. C., García-Pintado, J., & Bates, P. D. (2012). Automatic near real-time selection of flood water levels from high resolution Synthetic Aperture Radar images for assimilation into hydraulic models: A case study. *Remote Sensing of Environment*, 124, 705–716. <https://doi.org/10.1016/j.rse.2012.06.017>
- Matgen, P., Montanari, M., Hostache, R., Pfister, L., Hoffmann, L., Plaza, D., et al. (2010). Towards the sequential assimilation of SAR-derived water stages into hydraulic models using the Particle Filter: Proof of concept. *Hydrology and Earth System Sciences*, 14(9), 1773–1785. <https://doi.org/10.5194/hess-14-1773-2010>

- Mersel, M. K., Smith, L. C., Andreadis, K. M., & Durand, M. T. (2013). Estimation of river depth from remotely sensed hydraulic relationships. *Water Resources Research*, *49*, 3165–3179. <https://doi.org/10.1002/wrcr.20176>
- Moody, J. A., & Troutman, B. M. (2002). Characterization of the spatial variability of channel morphology. *Earth Surface Processes and Landforms*, *27*(12), 1251–1266. <https://doi.org/10.1002/esp.403>
- Mueller, N., Lewis, A., Roberts, D., Ring, S., Melrose, R., Sixsmith, J., et al. (2016). Water observations from space: Mapping surface water from 25 years of Landsat imagery across Australia. *Remote Sensing of Environment*, *174*, 341–352. <https://doi.org/10.1016/j.rse.2015.11.003>
- Neal, J., Keef, C., Bates, P., Beven, K., & Leedal, D. (2013). Probabilistic flood risk mapping including spatial dependence. *Hydrological Processes*, *27*(9), 1349–1363. <https://doi.org/10.1002/hyp.9572>
- Neal, J., Schumann, G., & Bates, P. (2012). A subgrid channel model for simulating river hydraulics and floodplain inundation over large and data sparse areas. *Water Resources Research*, *48*, W11506. <https://doi.org/10.1029/2012WR012514>
- Neal, J. C., Bates, P. D., Fewtrell, T. J., Hunter, N. M., Wilson, M. D., & Horritt, M. S. (2009). Distributed whole city water level measurements from the Carlisle 2005 urban flood event and comparison with hydraulic model simulations. *Journal of Hydrology*, *368*(1), 42–55. <https://doi.org/10.1016/j.jhydrol.2009.01.026>
- Neal, J. C., Fewtrell, T. J., Bates, P. D., & Wright, N. G. (2010). A comparison of three parallelisation methods for 2D flood inundation models. *Environmental Modelling & Software*, *25*(4), 398–411. <https://doi.org/10.1016/j.envsoft.2009.11.007>
- Neal, J. C., Odoni, N. A., Trigg, M. A., Freer, J. E., Garcia-Pintado, J., Mason, D. C., et al. (2015). Efficient incorporation of channel cross-section geometry uncertainty into regional and global scale flood inundation models. *Journal of Hydrology*, *529*, 169–183. <https://doi.org/10.1016/j.jhydrol.2015.07.026>
- Néelz, S., & Pender, G. (2013). *Benchmarking the latest generation of 2D hydraulic modelling packages* (Rep. SC120002). Bristol, UK: Environment Agency.
- O'Loughlin, F., Trigg, M. A., Schumann, G. J. P., & Bates, P. D. (2013). Hydraulic characterization of the middle reach of the Congo River. *Water Resources Research*, *49*, 5059–5070. <https://doi.org/10.1002/wrcr.20398>
- Orlandini, S., & Rosso, R. (1998). Parameterization of stream channel geometry in the distributed modeling of catchment dynamics. *Water Resources Research*, *34*(8), 1971–1985. <https://doi.org/10.1029/98WR00257>
- Ozdemir, H., Sampson, C. C., de Almeida, G. A. M., & Bates, P. D. (2013). Evaluating scale and roughness effects in urban flood modelling using terrestrial LIDAR data. *Hydrology and Earth System Sciences*, *17*(10), 4015–4030. <https://doi.org/10.5194/hess-17-4015-2013>
- Pagano, T. C., Wood, A. W., Ramos, M. H., Cloke, H. L., Pappenberger, F., Verkade, J. S., et al. (2014). *Challenges of operational river forecasting*. <https://doi.org/urn:NBN:nlui:24-uuid:92f5a520-c2f8-4afa-817e-ef75bfe20269>
- Pan, Z., Glennie, C., Legleiter, C., & Overstreet, B. (2015). Estimation of water depths and turbidity from hyperspectral imagery using support vector regression. *IEEE Geoscience and Remote Sensing Letters*, *12*(10), 2165–2169. <https://doi.org/10.1109/LGRS.2015.2453636>
- Pappenberger, F., Beven, K., Frodsham, K., Romanowicz, R., & Matgen, P. (2007). Grasping the unavoidable subjectivity in calibration of flood inundation models: A vulnerability weighted approach. *Journal of Hydrology*, *333*(2–4), 275–287. <https://doi.org/10.1016/j.jhydrol.2006.08.017>
- Pasternack, G. B., & Senter, A. E. (2011). *21st Century instream flow assessment framework for mountain streams*. California Energy Commission.
- Pavelsky, T. M., & Smith, L. C. (2008). RivWidth: A software tool for the calculation of river widths from remotely sensed imagery. *IEEE Geoscience and Remote Sensing Letters*, *5*(1), 70–73. <https://doi.org/10.1109/LGRS.2007.908305>
- Perez, J. F., Swain, N. R., Dolder, H. G., Christensen, S. D., Snow, A. D., Nelson, E. J., et al. (2016). From global to local: providing actionable flood forecast information in a cloud-based computing environment. *JAWRA Journal of the American Water Resources Association*, *52*(4), 965–978. <https://doi.org/10.1111/1752-1688.12392>
- Phillips, J. D. (1990). The instability of hydraulic geometry. *Water Resources Research*, *26*(4), 739–744. <https://doi.org/10.1029/WR026i004p00739>
- Rodriguez, E. (2015). *Surface Water and Ocean Topography mission (SWOT), Science Requirements document*. Retrieved from https://swot.jpl.nasa.gov/files/swot/SRD_021215.pdf
- Rosgen, D. L. (1996). *Applied river morphology*. Fort Collins, CO: Wildland Hydrology.
- Sampson, C. C., Smith, A. M., Bates, P. D., Neal, J. C., Alfieri, L., & Freer, J. E. (2015). A high-resolution global flood hazard model. *Water Resources Research*, *51*, 7358–7381. <https://doi.org/10.1002/2015WR016954>
- Samuels, P. (1990). *Cross section location in one-dimensional models*. Paper presented at the International Conference on River Flood Hydraulics, Wallingford, UK.
- Savage, J. T. S., Bates, P., Freer, J., Neal, J., & Aronica, G. (2016a). When does spatial resolution become spurious in probabilistic flood inundation predictions?. *Hydrological Processes*, *30*(13), 2014–2032. <https://doi.org/10.1002/hyp.10749>
- Savage, J. T. S., Pianosi, F., Bates, P., Freer, J., & Wagener, T. (2016b). Quantifying the importance of spatial resolution and other factors through global sensitivity analysis of a flood inundation model. *Water Resources Research*, *52*, 9146–9163. <https://doi.org/10.1002/2015WR018198>
- Schumann, G., Neal, J. C., Voisin, N., Andreadis, K. M., Pappenberger, F., Phanthuwongpakdee, N., et al. (2013). A first large-scale flood inundation forecasting model. *Water Resources Research*, *49*, 6248–6257. <https://doi.org/10.1002/wrcr.20521>
- Schumann, G. J. P., Andreadis, K. M., & Bates, P. D. (2014). Downscaling coarse grid hydrodynamic model simulations over large domains. *Journal of Hydrology*, *508*, 289–298. <https://doi.org/10.1016/j.jhydrol.2013.08.051>
- Schumann, G. J. P., Bates, P. D., Neal, J. C., & Andreadis, K. M. (2015). Chapter 2 - Measuring and mapping flood processes. In J. F. S. P. D. Bal-dassarre (Ed.), *Hydro-meteorological hazards, risks and disasters* (pp. 35–64). Boston, MA: Elsevier.
- Schumann, G. J. P., Stampoulis, D., Smith, A. M., Sampson, C. C., Andreadis, K. M., Neal, J. C., et al. (2016). Rethinking flood hazard at the global scale. *Geophysical Research Letters*, *43*, 10249–10256. <https://doi.org/10.1002/2016GL070260>
- Sene, K. (2008). *Flood warning, forecasting and emergency response*. Berlin, Germany: Springer.
- Soar, P., Wallerstein, N., & Thorne, C. (2017). Quantifying river channel stability at the basin scale. *Water*, *9*(2), 133.
- Stephens, E., & Bates, P. (2015). Assessing the reliability of probabilistic flood inundation model predictions. *Hydrological Processes*, *29*(19), 4264–4283. <https://doi.org/10.1002/hyp.10451>
- Stephens, E., Schumann, G., & Bates, P. (2014). Problems with binary pattern measures for flood model evaluation. *Hydrological Processes*, *28*(18), 4928–4937. <https://doi.org/10.1002/hyp.9979>
- Stephens, E. M., Bates, P. D., Freer, J. E., & Mason, D. C. (2012). The impact of uncertainty in satellite data on the assessment of flood inundation models. *Journal of Hydrology*, *414–415*, 162–173. <https://doi.org/10.1016/j.jhydrol.2011.10.040>
- Stewardson, M. (2005). Hydraulic geometry of stream reaches. *Journal of Hydrology*, *306*(1), 97–111. <https://doi.org/10.1016/j.jhydrol.2004.09.004>

- Syme, W. (1991). *Dynamically linked two dimensional/one-dimensional hydrodynamic modelling program for rivers, estuaries and coastal waters* (master's thesis). St Lucia, Australia: The University of Queensland.
- Tourian, M. J., Tarpanelli, A., Elmi, O., Qin, T., Brocca, L., Moramarco, T., et al. (2016). Spatiotemporal densification of river water level time series by multimission satellite altimetry. *Water Resources Research*, *52*, 1140–1159. <https://doi.org/10.1002/2015WR017654>
- Trigg, M. A., Bates, P. D., Wilson, M. D., Schumann, G., & Baugh, C. (2012). Floodplain channel morphology and networks of the middle Amazon River. *Water Resources Research*, *48*, W10504. <https://doi.org/10.1029/2012WR011888>
- Trigg, M. A., Wilson, M. D., Bates, P. D., Horritt, M. S., Alsdorf, D. E., Forsberg, B. R., et al. (2009). Amazon flood wave hydraulics. *Journal of Hydrology*, *374*(1–2), 92–105. <https://doi.org/10.1016/j.jhydrol.2009.06.004>
- Twele, A., Cao, W., Plank, S., & Martinis, S. (2016). Sentinel-1-based flood mapping: A fully automated processing chain. *International Journal of Remote Sensing*, *37*(13), 2990–3004. <https://doi.org/10.1080/01431161.2016.1192304>
- Vermont Agency of Natural Resources. (2009). *Vermont stream geomorphic assessment*. Retrieved from <http://dec.vermont.gov/sites/dec/files/wsm/rivers/docs/assessment-protocol-appendices/K-Appendix-K-04-Identification-of-Bankfull-Stage.pdf>
- Waddle, T. (2010). Field evaluation of a two-dimensional hydrodynamic model near boulders for habitat calculation. *River Research and Applications*, *26*(6), 730–741. <https://doi.org/10.1002/rra.1278>
- Werner, M., Blazkova, S., & Petr, J. (2005). Spatially distributed observations in constraining inundation modelling uncertainties. *Hydrological Processes*, *19*(16), 3081–3096. <https://doi.org/10.1002/hyp.5833>
- Wood, M., Hostache, R., Neal, J., Wagener, T., Giustarini, L., Chini, M., et al. (2016). Calibration of channel depth and friction parameters in the LISFLOOD-FP hydraulic model using medium-resolution SAR data and identifiability techniques. *Hydrology and Earth System Sciences*, *20*(12), 4983–4997. <https://doi.org/10.5194/hess-20-4983-2016>
- Yamazaki, D., de Almeida, G. A. M., & Bates, P. D. (2013). Improving computational efficiency in global river models by implementing the local inertial flow equation and a vector-based river network map. *Water Resources Research*, *49*, 7221–7235. <https://doi.org/10.1002/wrcr.20552>
- Yamazaki, D., O'Loughlin, F., Trigg, M. A., Miller, Z. F., Pavelsky, T. M., & Bates, P. D. (2014). Development of the global width database for large rivers. *Water Resources Research*, *50*, 3467–3480. <https://doi.org/10.1002/2013WR014664>
- Yamazaki, D., Trigg, M. A., & Ikeshima, D. (2015). Development of a global ~ 90 m water body map using multi-temporal Landsat images. *Remote Sensing of Environment*, *171*, 337–351. <https://doi.org/10.1016/j.rse.2015.10.014>
- Yoon, Y., Durand, M., Merry, C. J., Clark, E. A., Andreadis, K. M., & Alsdorf, D. E. (2012). Estimating river bathymetry from data assimilation of synthetic SWOT measurements. *Journal of Hydrology*, *464*, 363–375. <https://doi.org/10.1016/j.jhydrol.2012.07.028>
- Yu, D., & Lane, S. N. (2006). Urban fluvial flood modelling using a two-dimensional diffusion-wave treatment, part 1: Mesh resolution effects. *Hydrological Processes*, *20*(7), 1541–1565. <https://doi.org/10.1002/hyp.5935>